New intermediate models for rotating shallow water and an investigation of the preference for anticyclones

MARK REMMEL[1] AND LESLIE SMITH[2]†

[1]Department of Mathematics, University of Wisconsin, Madison, WI 53706, USA

[2]Departments of Mathematics and Engineering Physics, University of Wisconsin, Madison, WI 53706, USA

New intermediate models for the rotating shallow water (RSW) equations are derived by considering the nonlinear interactions between subsets of the eigenmodes for the linearized equations. It is well-known that the two-dimensional quasi-geostrophic (QG) equation results when the nonlinear interactions are restricted to include only the vortical eigenmodes. Continuing past QG in a non-perturbative manner, the new models result by including subsets of interactions which include inertial-gravity wave (IG) modes. The such simplest model adds nonlinear interactions between one IG mode and two vortical modes. In sharp contrast to QG, the latter model behaves similar to the full RSW equations for decay from balanced initial conditions as well as unbalanced random initial conditions with divergence-free velocity. Quantitative agreement is observed for statistics that measure structure size, intermittency and cyclone/anticyclone asymmetry. In particular, dominance of anticyclones is observed for Rossby numbers Ro in the range $0.1 < Ro < 1$ (away from the QG parameter regime $Ro \to 0$). A hierarchy of models is explored to determine the effects of wave-vortical and wave–wave interactions on statistics such as the skewness of vorticity in decaying turbulence. Possible advantages over previously derived intermediate models include (i) the non-perturbative nature of the new models (not restricting them *a priori* to any particular parameter regime) and (ii) insight into the physical and mathematical consequences of vortical–wave interactions.

1. Introduction

The equation sets governing geophysical flows involve the complex interaction of (nonlinear) waves and turbulence over a vast range of space and time scales. Depending on the atmospheric or oceanic processes of interest, the starting point for analysis and/or computation of the fluid dynamics may be the rotating shallow water (RSW) equations (Pedlosky 1986; Salmon 1998), the rotating Boussinesq equations (RBE) (Salmon 1998; Majda 2003; Kundu & Cohen 2004) or the primitive equations (PE) (Salmon 1998). Each system of partial differential equations is characterized by a linear operator giving rise to wave eigenmodes in the linear (inviscid) limit, and a quadratic nonlinear operator leading to mode coupling in both space and time. For both practical and theoretical purposes, it is often advantageous to have simpler models that exclude some physics (usually the fast small-scale motions). For

† Email address for correspondence: lsmith@math.wisc.edu

example, before computers made it feasible to numerically integrate the full equation sets, it was desirable to have a simpler equation describing the evolution of slow large-scale motions contributing to weather on relatively short time scales (several days). Charney's (1948) quasi-geostrophic (QG) equation fits that role. Charney derived the QG model using physically relevant and insightful scaling arguments (Charney 1948; Obukhov 1949), and the QG model may also be obtained from an asymptotic expansion (Pedlosky 1986). The QG equation is void of gravity waves and therefore allowed a much larger time step in early computations (Salmon 1998). In addition, QG requires initial data for only one variable (the pseudo-potential vorticity). The classical QG equation is perhaps best suited for mid-latitude planetary scale motion partly because of the 'thin-layer' assumption used in its derivation. The use of this assumption limits the scale of the vertical velocity. Recently, analogous reduced equations have been derived that pertain to other geophysically relevant regimes (Julien *et al.* 2006), for example, those having a vertical scale equal to or greater than the horizontal scale allowing for increased vertical motion.

However, important features of geophysical flows are missed by QG dynamics. Several books discuss methods to correct QG used for weather prediction (e.g. Martin 2006). Attempts to include physics beyond QG naturally involved formally extending the asymptotic analysis to next order. Various 'intermediate models' arise from different assumptions and goals as higher-order corrections to QG are determined. Intermediate models attempt to improve upon the two-dimensional QG equation derived from RSW (Allen, Barth & Newberger 1990*a*; Spall & McWilliams 1992; Yavneh & McWilliams 1994; Warn *et al.* 1995; Vallis 1996, and cited literature), as well as upon the analogous three-dimensional QG equation derived from the three-dimensional RBE (or equivalently from the three-dimensional PE) (Allen 1991, 1993; Muraki, Snyder & Rotunno 1999; Muraki & Hakim 2001, and cited references). For example, intermediate models for RSW have been used to numerically study flows over $O(1)$ topography (Barth, Allen & Newberger 1990) and boundary trapped waves (Allen, Barth & Newberger 1990*b*). For these cases QG is not formally valid (process violates a derivation assumption), filters out the motions of interest and/or is inaccurate. These studies, applied to oceanographic flow off the west coast of the United States, found that certain so-called 'balance equation' intermediate models performed the best in the sense of accuracy (Allen *et al.* 1990*b*; Barth *et al.* 1990).

Some intermediate models maintain analogues of conserved volume integrals and of the Lagrangian invariant potential vorticity (PV) of the original equations, others maintain one of the two and others lose both (see table 1 of Allen *et al.* 1990*a* for RSW and §3 of Allen & Newberger 1993 for PE). For RBE and RSW, PV is the scalar product of the absolute vorticity and the gradient of a conserved quantity. The conserved quantity generally used for RBE is the density (Majda 2003). For RSW the conserved quantity is $(z - h_B)/D$, where z is the vertical coordinate, h_B is the height of the bottom topography and D is the total depth of the fluid layer between the free surface and the bottom topography (Pedlosky 1986). Many studies have attempted to determine the relative importance of PV conservation and/or global energy conservation (e.g. McWilliams & Gent 1980). For example, considering RSW, Allen *et al.* (1990*a*) found that particular intermediate models maintaining only PV conservation performed better than other models with both PV and global energy conservation. Previously, two similar finite-difference algorithms were tested for the non-rotating shallow water equations (Sadourny 1975). The algorithms differ only in the space averaging of the non-gradient part of the nonlinear term of the momentum equations, leading one numerical model to conserve energy but not potential enstrophy

and vice-versa for the other numerical model. It was found that the energy-conserving scheme violated basic flow properties of shallow water in the scale transfer of energy (non-divergent part) and enstrophy. This perhaps started the evidence that potential enstrophy conservation is more important to maintain than energy conservation in shallow water numerical models.

The conserved quantities maintained by an intermediate model are not necessarily predetermined by the derivation procedure. For instance, the balance equations (BEs) result from truncation at $O(\epsilon)$ of the equations for the vertical component of vorticity and the horizontal velocity divergence, where ϵ is the Rossby number (Ro) measuring the ratio of rotational and nonlinear time scales. For RSW this procedure leads to an intermediate model with a Lagrangian invariant analogous to PV, whereas for the PE, the intermediate model has a volume integral analogous to energy conservation (Lorenz 1960; Allen 1991). Partly to maintain an analogue to the PV as an invariant, the balance equations based on momentum (BEM) retain explicit momentum equations (Allen 1991). The BEM and BE models differ by a few higher-order terms in their respective balance equations, but the BEM has analogues of both PV and global energy conservation. Numerical experiments for the time evolution of an unstable baroclinic jet using BE, BEM and other intermediate models have shown that neither exact conservation of PV nor volume integrals of an energy density are crucial for accuracy in the mesoscale parameter range (Allen & Newberger 1993).

In Warn *et al.* (1995) it is shown that expanding all variables in the relevant small parameter can and does lead to secularities in higher-order expansions beyond QG. An iterative approach, free from secular terms, has been developed and the resulting models asymptotically conserve PV and energy (see Allen 1993; Allen & Newberger 1993). Another technique which avoids secular terms designates a 'distinguished evolution variable', related to the slow modes, and expands the fast modes only (typically with the Rossby number or Froude number as the small parameter). The PV has been used as the distinguished variable because of its slow nature (other variables that project onto the slow modes are also used) for both RSW and PE (Warn *et al.* 1995; Vallis 1996). As stated by Vallis (1996), models derived in this way are not guaranteed to exactly maintain the integral invariants of mass and energy.

The works by Muraki *et al.* (1999) and McIntyre & Norton (2000) are related balance models similar to each other in their methodology, and to the papers discussed in the previous paragraph. In both, the prognostic equation is advection of the (unexpanded) Lagrangian invariant PV. The work by Muraki *et al.* (1999) extends QG for the PE on the f-plane with the region bounded at the bottom and the top by horizontal surfaces. The formulation is in physical space and employs a change of variables that exploits the gradient-like structure between the flow variables and the pressure at first order in Ro. QG is readily obtained by neglecting $O(1)$ contributions in the expansion. Hence, there is a natural separation between the balanced flow and gravity waves. Furthermore, extension of the model to next order is straightforward. The PV is temporarily expanded in Ro according to solvability constraints derived from its conserved volume integral in order to invert for the corresponding order gradient scalar potential. While PV conservation holds to all orders, other conserved relations are only approximate with error determined by the accuracy of the expansion in powers of Ro. The resulting equations were tested by calculating the next order corrections to a finite amplitude Eady edge wave. The same intermediate model was then applied numerically to unstable waves on baroclinic jets (Rotunno, Muraki & Snyder 2000). A similarly derived model was used to study the asymmetry between cyclones and anticyclones on the tropopause by extending the surface QG model

(Hakim, Snyder & Muraki 2002). Repeating the procedure used in Muraki *et al.* (1999) for RBE within a periodic setting, it is straightforward to show that the gradient potential is related to the vortical mode and that the curl potentials are related to the IG modes. At $O(1)$, the curl potentials are obtained directly from the leading-order gradient potential alone, and hence the IG modes are determined by interactions with two vortical modes. In fact, the equations for the curl potentials are contained within the equations obtained by neglecting the time derivative of the IG modes and considering only the interactions involving two vortical modes to force the IG modes. Thus, the Muraki *et al.* (1999) model has aspects related to the model denoted by PPG derived herein, which includes all three-mode interactions involving two or three vortical modes.

In the work by McIntyre & Norton (2000), normal-mode PV inversion balance models were developed pertaining to RSW on a hemisphere and RSW on the f-plane. These models are surprisingly accurate as noted by McIntyre and Norton themselves. For decay from initial conditions containing a small percentage of gravity waves, the third-order normal-mode inversion model yielded height fields in remarkable agreement with the corresponding height fields attained by integrating the full equations for considerable periods of time. The good agreement was robust even when the flows had regions where the Fr or Ro were far from zero. The normal-mode inversion models 'slave' the IG-mode amplitudes directly to the PV. First, the vortical-mode amplitudes are calculated in an iteration process via a relation involving linear PV and the true PV anomaly. Next, the IG mode amplitudes are updated by either neglecting (first order) or diagnostically estimating (higher order) the time derivatives of the IG mode amplitudes in the modal equivalent equations for RSW. This process is iterated (see McIntyre & Norton 2000, for the details). In contrast to Muraki *et al.* (1999) and our PPG model, the evolution of the IG modes results from all types of interactions with vortical modes and other IG modes. In our model hierarchy, we further dissect the normal-mode approach by isolating classes of interactions to evolve the IG-mode (and vortical mode) amplitudes. Our derivation procedure also leads naturally to physical space partial differential equations by way of inverse transform, or by starting from RSW or RBE rewritten in terms of appropriate physical variables.

Other than using an asymptotic expansion, the two-dimensional QG and three-dimensional QG equations can be obtained by considering nonlinear interactions among only the vortical linear eigenmodes, i.e. the modes corresponding to the 'slow' eigenvalue of the linearized RSW or RBE system (Salmon 1998; Smith & Waleffe 2002; Majda 2003). Our novel approach continues past two-dimensional QG or three-dimensional QG by also including subsets of inertial-gravity wave eigenmodes of RSW or RBE, respectively. Different intermediate models are derived by considering different subsets of the interactions along with the interaction among the vortical modes, and thus each model includes physics beyond two-dimensional QG or three-dimensional QG. These new intermediate models have all the wave frequencies of the full equations, some or all of which are either filtered out or altered by previous intermediate models. The new three-dimensional intermediate models for RBE naturally conserve energy by the properties of individual triad interactions (§3 of Kraichnan 1973, see also Appendix B); while energy conservation is not guaranteed for the new intermediate models beyond two-dimensional QG because of the cubic nature of the RSW energy. In fact, it is well known that energy conservation is an issue with any wavenumber truncation of the RSW equations (Warn 1986; Farge & Sadourny 1989; Yuan & Hamilton 1994). As discussed, lack of

strict energy conservation does not preclude computational accuracy for time scales of typical interest (Allen & Newberger 1993). In our numerical computations (with high-wavenumber dissipation), the energy as a function of time is well behaved, allowing us to draw conclusions regarding the role of wave–vortical mode interactions.

The focus of the present manuscript is on new intermediate models for RSW, and models for RBE will be presented elsewhere. Unlike previous intermediate models, our new models do not depend on a small parameter and hence may be more accurate in parameter regimes away from the two-dimensional QG regime corresponding to vanishing Rossby number. Models including vortical–IG wave mode interactions should be a natural way to study the coupling between the balanced and unbalanced components of the flow, a topic of much recent interest (Bartello 1995; Embid & Majda 1996, 1998; Majda & Embid 1998; Salmon 1998; Kuo & Polvani 1999; Ford, McIntyre & Norton 2000; Reznik, Zeitlin & Ben Jelloul 2001; Majda 2003). Based on an orthogonal eigenmode decomposition in wave space, the new partial differential equation models result after an inverse Fourier transform to physical space, and can be used with any appropriate physical-space boundary conditions. However, they often contain more nonlinear terms than the full equations, and often these nonlinear terms involve inverse operators. Hence, despite advantages, their role may be limited to promoting understanding as a research tool.

A particular shortcoming of QG is its inability to capture the asymmetry between cyclonic and anticyclonic vortices (Polvani *et al.* 1994; Kuo & Polvani 2000). This is to be expected mathematically since the QG equation is parity invariant. Cyclone/anticyclone asymmetry in geophysical flows and the equations that model them has received considerable attention (Polvani *et al.* 1994; Kuo & Polvani 2000; Rotunno *et al.* 2000; Muraki & Hakim 2001; Hakim *et al.* 2002). Observations show, for example, cyclone dominance in the tropospheric midlatitudes; a prevalence of anticyclones at oceanic mesoscales; and anticyclone dominance in the Jovian atmosphere (see, e.g. Kuo & Polvani 2000, and references therein). In two-dimensional, once the incompressibility constraint is broken (as in RSW) asymmetries develop. In RSW the asymmetry is in favour of anticyclones for moderately small values of the Rossby number, i.e. away from the geostrophic parameter regime corresponding to vanishing Rossby number (Polvani *et al.* 1994). For β-plane RSW, steady axisymmetric anticyclonic solutions were sought to equations derived from multiple scale asymptotic expansions in four regimes based on the ratio of the relevant small parameters. These steady axisymmetric anticyclonic solutions were found only in the so-called nonlinear QG regime with characteristic length scale much larger than the Rossby deformation radius and characteristic velocity scale much larger than the Rossby velocity (see Stegner & Zeitlin 1995).

Since the (symmetric) two-dimensional QG model involves only nonlinear interactions among vortical modes, interactions involving IG modes obviously have a role in the cyclone/anticyclone asymmetry. One aim of this work is to gain insight into which subset of mode interactions is most important for the generation of anticyclones in RSW decay from both balanced and unbalanced initial conditions.

The rotating shallow water RSW equations and their properties are given in §2, including a discussion of linear eigenmodes and nonlinear invariants. Intermediate models, including physics beyond QG, are developed in §3. Section 4 compares numerical results and statistics for RSW and some of the models. In §5, numerical results are presented for the model obtained by including only the nonlinear interactions among the IG eigenmodes. Conclusions and discussion are given in §6. Interaction coefficients are derived and listed in appendix A. A lemma regarding

energy conservation is given in appendix B. Fourier space representations for two of the models are presented in appendix C. Two of the reduced models in partial differential equation form are found in appendix D.

2. The rotating shallow water equations

The RSW equations can be written as

$$
\left.
\begin{aligned}
\frac{\partial u}{\partial t} + u\frac{\partial u}{\partial x} + v\frac{\partial u}{\partial y} - fv &= -g\frac{\partial h}{\partial x}, \\
\frac{\partial v}{\partial t} + u\frac{\partial v}{\partial x} + v\frac{\partial v}{\partial y} + fu &= -g\frac{\partial h}{\partial y}, \\
\frac{\partial h}{\partial t} + u\frac{\partial h}{\partial x} + v\frac{\partial h}{\partial y} + (H+h)\left(\frac{\partial u}{\partial x} + \frac{\partial v}{\partial y}\right) &= 0,
\end{aligned}
\right\}
\tag{2.1}
$$

where u is the velocity in the $\hat{\mathbf{x}}$-direction, v is the velocity in the $\hat{\mathbf{y}}$-direction, H is the mean depth, h is the perturbation from the mean H, the rotation axis is $\hat{\mathbf{z}}$, f is twice the constant rotation rate and g is the the acceleration due to gravity. Equations (2.1) have the Lagrangian invariant

$$
q = \frac{\nabla^2\Psi + f}{H+h},
\tag{2.2}
$$

called potential vorticity, where $\nabla^2\Psi = v_x - u_y$ is the vorticity and Ψ is the streamfunction. After linearizing q, the non-constant part leaves

$$
Q = \nabla^2\Psi - \frac{f}{H}h.
\tag{2.3}
$$

Quantity (2.3) will be referred to as linear PV in this paper. Equations (2.1) also have integral invariants in domains where the fluxes are zero or cancel, e.g. in periodic domains. One such invariant is the energy

$$
E = \frac{1}{2}\int_A \left((H+h)(u^2+v^2) + gh^2\right)\mathrm{d}A.
\tag{2.4}
$$

For scalar functions $r(q)$, another class of integral invariants has the form

$$
S(r) = \frac{1}{2}\int_A (H+h)r(q)\,\mathrm{d}A.
\tag{2.5}
$$

When r is the square function, this invariant is called potential enstrophy.

Notice that energy and potential enstrophy for RSW are not quadratic, a well-known difficulty with the shallow water equations. The cubic nature of the RSW energy and potential enstrophy means that these invariants are not strict under a truncation in spectral space (Warn 1986; Farge & Sadourny 1989; Yuan & Hamilton 1994), and their conservation is not guaranteed by our reduced models. Numerically, however, the energy of the models is well behaved during decay (see figure 1). For the RBE the appropriately defined energy is quadratic and strictly conserved by spectral space truncation or restriction of triad (and mode) interactions. Thus, new intermediate RBE models derived from subsets of triad mode interactions automatically conserve energy (see appendix B).

It is convenient to rewrite (2.1) so that the Fourier transform of its linear part is in skew-hermitian form. The first two equations may be multiplied by $\sqrt{H}$, and the
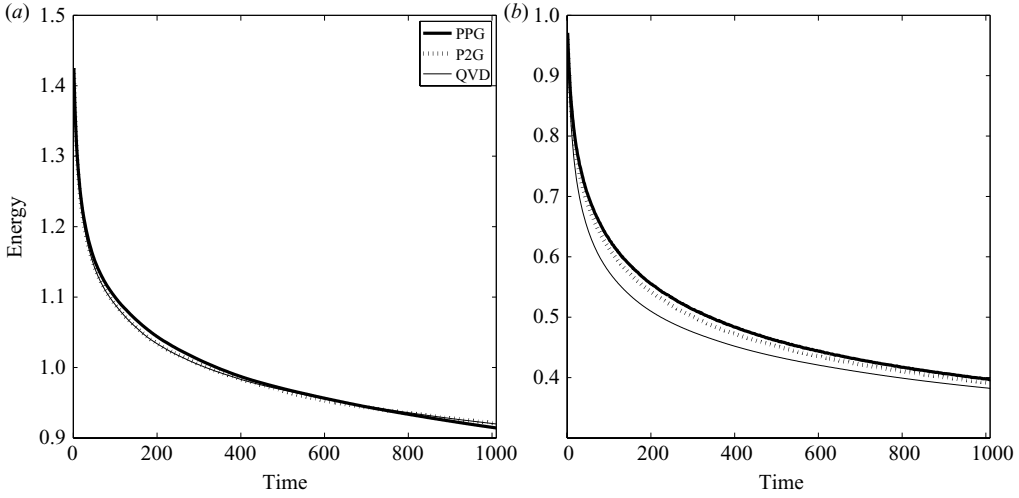
FIGURE 1. Representative plots of energy versus time for $Ro = .25$ and $Fr = .2$. (*a*) Balanced initial conditions. (*b*) Unbalanced initial conditions (A100).

third equation by $\sqrt{g}$, to arrive at,

$$
\left.
\begin{aligned}
&\frac{\partial \psi_1}{\partial t} + \frac{1}{\sqrt{H}}\left(\psi_1\frac{\partial \psi_1}{\partial x} + \psi_2\frac{\partial \psi_1}{\partial y}\right) - f\psi_2 = -c\frac{\partial \psi_3}{\partial x}, \\
&\frac{\partial \psi_2}{\partial t} + \frac{1}{\sqrt{H}}\left(\psi_1\frac{\partial \psi_2}{\partial x} + \psi_2\frac{\partial \psi_2}{\partial y}\right) + f\psi_1 = -c\frac{\partial \psi_3}{\partial y}, \\
&\frac{\partial \psi_3}{\partial t} + \frac{1}{\sqrt{H}}\left(\psi_1\frac{\partial \psi_3}{\partial x} + \psi_2\frac{\partial \psi_3}{\partial y} + \psi_3\left(\frac{\partial \psi_1}{\partial x} + \frac{\partial \psi_2}{\partial y}\right)\right) + c\left(\frac{\partial \psi_1}{\partial x} + \frac{\partial \psi_2}{\partial y}\right) = 0,
\end{aligned}
\right\}
\quad (2.6)
$$

where $(\psi_1, \psi_2) = \sqrt{H}(u, v)$ and $\psi_3 = \sqrt{g}h$ (Salmon 1998). In addition, $c = \sqrt{gH}$, the non-rotating shallow water wave speed. In terms of the new variables, integral invariant (2.4) may be written as $E = E_{quad} + E_{cubic}$, where

$$
E_{quad} = \frac{1}{2}\int_A \left(\psi_1^2 + \psi_2^2 + \psi_3^2\right) \mathrm{d}A
\quad (2.7)
$$

and

$$
E_{cubic} = \frac{1}{2}\int_A \frac{1}{\sqrt{gH}}\psi_3\left(\psi_1^2 + \psi_2^2\right) \mathrm{d}A.
\quad (2.8)
$$

For many flows E_{quad} is the dominant contributor to the total energy, in particular for small amplitude flows. For flows of the latter nature, it is easy to show that the potential enstrophy also has a dominant quadratic contribution. Hence, for weak motions these quadratic psuedo-constraints have been used to represent energy and potential enstrophy (Warn 1986; Farge & Sadourny 1989; Yuan & Hamilton 1994), allowing space scale separation (by wavenumber). Moreover, even though RSW allows self-interactions, it still satisfies the Liouville property (Warn 1986, page 4), and thereby the quadratic invariants allows the use of statistical mechanics to obtain an equipartition distribution for the vortical and IG mode amplitudes (see Warn 1986, for the details and references therein). Even though the energy for RBE is quadratic, the appropriately defined potential enstrophy can only be taken as quadratic for small

amplitude flows as well. In this case, as for RSW, an equipartition distribution has been derived (Bartello 1995).

For an unbounded or periodic domain, the linear eigenmodes of (2.6) are Fourier modes

$$\boldsymbol{\psi}(\boldsymbol{x}, t) = \boldsymbol{\phi}(\boldsymbol{k})e^{i(\boldsymbol{k}\cdot\boldsymbol{x}-\omega(\boldsymbol{k})t)}. \tag{2.9}$$

It can be shown from the linear limit of PV conservation that either $\omega = 0$ or the mode has no linear PV (see Bartello 1995, for the analogous Boussinesq result). This fact can also be seen directly from the explicit eigenfunctions.

Substituting (2.9) into the linearized form of (2.6) leads to

$$\omega^0 = 0, \quad \omega^+ = +\sqrt{f^2 + c^2 k^2}, \quad \omega^- = -\sqrt{f^2 + c^2 k^2}, \tag{2.10}$$

where $k = |\boldsymbol{k}| = \sqrt{\boldsymbol{k}_{\boldsymbol{x}}^2 + \boldsymbol{k}_{\boldsymbol{y}}^2} = \boldsymbol{0}$. The corresponding orthonormal eigenfunctions are

$$\boldsymbol{\phi}^0 = \frac{1}{\omega}\begin{pmatrix} -ik_y c \\ ik_x c \\ f \end{pmatrix}, \boldsymbol{\phi}^{\pm} = \frac{1}{\sqrt{2}\omega k}\begin{pmatrix} \pm\omega k_x + ifk_y \\ \pm\omega k_y - ifk_x \\ c(k_x^2 + k_y^2) \end{pmatrix}, \tag{2.11}$$

where $\omega = \sqrt{f^2 + c^2 k^2}$. For the special case $k = 0$,

$$\omega^0 = 0, \quad \omega^+ = f, \quad \omega^- = -f, \tag{2.12}$$

with corresponding eigenfunctions (pure inertial modes $\boldsymbol{\phi}^+$ and $\boldsymbol{\phi}^-$)

$$\boldsymbol{\phi}^0 = \begin{pmatrix} 0 \\ 0 \\ 1 \end{pmatrix}, \quad \boldsymbol{\phi}^+ = \frac{1}{\sqrt{2}}\begin{pmatrix} i \\ 1 \\ 0 \end{pmatrix}, \quad \boldsymbol{\phi}^- = \frac{1}{\sqrt{2}}\begin{pmatrix} -i \\ 1 \\ 0 \end{pmatrix}. \tag{2.13}$$

These modes ($\boldsymbol{\phi}^{\alpha}e^{i\boldsymbol{k}\cdot\boldsymbol{x}}$, $\alpha = 0, +, -$, for all $\boldsymbol{k}$) form a complete set of functions (Salmon 1998). Therefore, in the derivation of the models and parts of the numerical computations, the nonlinear solution is expanded as

$$\boldsymbol{\psi}(\boldsymbol{x}, t) = \sum_{\boldsymbol{k}}(a^0(\boldsymbol{k}, t)\boldsymbol{\phi}^0 + a^+(\boldsymbol{k}, t)\boldsymbol{\phi}^+ + a^-(\boldsymbol{k}, t)\boldsymbol{\phi}^-)e^{i\boldsymbol{k}\cdot\boldsymbol{x}}. \tag{2.14}$$

The Fourier-transform of (2.6) then becomes

$$\frac{\partial a_{\boldsymbol{k}}^0}{\partial t}\boldsymbol{\phi}_{\boldsymbol{k}}^0 + \frac{\partial a_{\boldsymbol{k}}^+}{\partial t}\boldsymbol{\phi}_{\boldsymbol{k}}^+ + \frac{\partial a_{\boldsymbol{k}}^-}{\partial t}\boldsymbol{\phi}_{\boldsymbol{k}}^- + i\omega_{\boldsymbol{k}}^0 a_{\boldsymbol{k}}^0\boldsymbol{\phi}_{\boldsymbol{k}}^0 + i\omega_{\boldsymbol{k}}^+ a_{\boldsymbol{k}}^+\boldsymbol{\phi}_{\boldsymbol{k}}^+ + i\omega_{\boldsymbol{k}}^- a_{\boldsymbol{k}}^-\boldsymbol{\phi}_{\boldsymbol{k}}^- = -\widehat{NL}_{\boldsymbol{k}} \tag{2.15}$$

where

$$\widehat{NL}_{\boldsymbol{k}} = \frac{1}{\sqrt{H}}\begin{pmatrix} \widehat{\psi_1\psi_{1x} + \psi_2\psi_{1y}} \\ \widehat{\psi_1\psi_{2x} + \psi_2\psi_{2y}} \\ \widehat{\psi_1\psi_{3x} + \psi_2\psi_{3y} + \psi_3(\psi_{1x} + \psi_{2y})} \end{pmatrix}_{\boldsymbol{k}} \tag{2.16}$$

and a hat denotes Fourier transform. The time evolution equation for $a_{\boldsymbol{k}}^{\alpha}$ ($\alpha = 0, +, $ or $-$) is obtained after scalar product of (2.15) by $\overline{\boldsymbol{\phi}_{\boldsymbol{k}}^{\alpha}}$, where an overbar means complex conjugate, and using orthonormality,

$$\frac{\partial a_{\boldsymbol{k}}^{\alpha}}{\partial t} + i\omega_{\boldsymbol{k}}^{\alpha} a_{\boldsymbol{k}}^{\alpha} = -\widehat{NL}_{\boldsymbol{k}} \cdot \overline{\boldsymbol{\phi}_{\boldsymbol{k}}^{\alpha}}. \tag{2.17}$$

Notice that reality implies the following conditions for the amplitudes:

$$a^0(\boldsymbol{k}) = \overline{a^0(-\boldsymbol{k})}, \quad a^+(\boldsymbol{k}) = \overline{a^-(-\boldsymbol{k})}, \quad a^-(\boldsymbol{k}) = \overline{a^+(-\boldsymbol{k})} \text{ and } a^-(\boldsymbol{0}) = \overline{a^+(\boldsymbol{0})}, \tag{2.18}$$

which are useful in deriving the interaction coefficients and hence the models.

3. Models

Through quadratic term (2.16), two modes $\boldsymbol{\phi}_p^\beta$ and $\boldsymbol{\phi}_q^\gamma$ can interact to force a third mode $\boldsymbol{\phi}_k^\alpha$, where α, β and γ can be 0, $+$ or $-$ for triad interactions with $\boldsymbol{k} = \boldsymbol{p} + \boldsymbol{q}$. We shall represent such an interaction as $\alpha|\beta\gamma$ and the interaction coefficient by $C_{kpq}^{\alpha\beta\gamma}$. The right-hand side of (2.17) involves a sum of β and γ over $0, +, -$. New models are obtained by restricting the sum and allowing only certain mode interactions. For instance, α, β and γ can all be restricted to the 0 (vortical) mode. In this case there is only one time evolution equation to invert and the two-dimensional QG equation results. Calculation of an interaction coefficient is demonstrated in appendix A and the explicit results are listed.

Since the velocity of the RSW equations is not divergence free, a mean flow can be generated even when not present initially (Warn 1986; Yuan & Hamilton 1994). This fact manifests itself in Fourier space by non-zero interaction coefficients involving the mean flows (Warn 1986, see appendix A) of the form $C_{0k-k}^{s\beta\gamma}$, where s is $+$ or $-$. On the other hand, by (2.13), $a_{k=0}^0$ is proportional to $h_{k=0}$. Hence, its time derivative is zero. This can be seen by averaging the h equation of (2.1) (conservation of mass). Moreover, it is easy to check that $C_{0k-k}^{0\beta\gamma}$ is zero for all combinations of β and γ. It is natural to take the constant $a_{k=0}^0 = 0$ (it will remain zero for all models).

The generation of mean flows in RSW can possibly affect the dynamics in a non-trivial way. For completeness, every model is given with all mean flow contributions. However, all numerical work done on the models excluded these mean flow additions. For consistency, the mean flows were set to zero at every time step for the full RSW equations (2.6) in all the numerical results reported in this paper.

3.1. *Quasi-geostrophy*

As mentioned, it is well-known that when the vortical modes alone are used to represent $\boldsymbol{\psi}$ in (2.14), an inverse Fourier-transform of (2.17) gives one derivation of the two-dimensional QG equation (Salmon 1998). The reader familiar with this derivation of the two-dimensional QG model may skip §3.2. In this case (2.14) gives

$$\sqrt{H}k^2\Psi_k = \frac{a_k^0}{\omega_k}k^2c \qquad \text{and} \qquad \sqrt{g}k^2h_k = \frac{a_k^0}{\omega_k}k^2f \tag{3.1}$$

so that after a little algebra

$$f\Psi = gh \qquad \text{and} \qquad a_k^0 = \frac{\omega_k\Psi}{\sqrt{g}}, \tag{3.2}$$

where Ψ is the streamfunction and the first relation of (3.2) is called geostrophic balance. Also, in this case (2.17) has only the equation

$$\frac{\partial a_k^0}{\partial t} = \frac{1}{\sqrt{H}} \sum_{k+p+q=0} \frac{\overline{a_p^0 a_q^0}}{\omega_p\omega_q\omega_k}c(\boldsymbol{q} \times \boldsymbol{p} \cdot \hat{z})\left(\frac{\omega_p^2 - \omega_q^2}{2}\right). \tag{3.3}$$

Substituting (3.2) into (3.3) and bringing the result back to physical space obtains

$$\frac{\partial Q}{\partial t} + J(\Psi, Q) = 0, \tag{3.4}$$

where $Q = (\nabla^2 - f^2/gH)\Psi$ is the linear PV (2.3) when there is geostrophic balance and $J(f, g) = f_x g_y - f_y g_x$ is the Jacobian. There are no mean flow additions to two-dimensional QG.

3.2. *Models with gravity wave modes*

A primary goal of this work is to understand how IG modes interact with vortical modes and with each other, leading to a departure from QG dynamics. Therefore, models are developed including interactions involving IG modes. These models have, in addition to an evolution equation for a_k^0, evolution equations for a_k^+ and a_k^-. Further the geostrophic relation between Ψ and h is broken, and the relationship between a_k^0, a_k^+, a_k^- and u, v, h (or Ψ, χ, $\langle u \rangle$, $\langle v \rangle$, h) must be ascertained, where χ is the potential function and $\langle \cdot \rangle$ denotes a domain average ($u = \chi_x - \Psi_y + \langle u \rangle$, $v = \chi_y + \Psi_y + \langle v \rangle$, $\nabla^2 \chi = u_x + v_y$). For $k \neq 0$, the relation is

$$\begin{pmatrix} \sqrt{H}(\mathrm{i}k_x\chi - \mathrm{i}k_y\Psi) \\ \sqrt{H}(\mathrm{i}k_y\chi + \mathrm{i}k_x\Psi) \\ \sqrt{g}h_k \end{pmatrix} = a^0(\boldsymbol{k}, t)\boldsymbol{\phi}_k^0 + a^+(\boldsymbol{k}, t)\boldsymbol{\phi}_k^+ + a^-(\boldsymbol{k}, t)\boldsymbol{\phi}_k^-. \tag{3.5}$$

Using the orthonormality of the eigenmodes and adding and subtracting the result for a_k^+ and a_k^- yields

$$a_k^0 = \frac{-c\sqrt{H}}{\omega_k}\left(-k^2\Psi_k - \frac{f}{H}h_k\right) = \frac{-c\sqrt{H}}{\omega_k}Q_k, \tag{3.6}$$

$$a_k^+ + a_k^- = \frac{\sqrt{2}\sqrt{H}k}{\omega_k}(-f\Psi_k + gh_k) = -\frac{\sqrt{2}\sqrt{H}k}{\omega_k}V_k, \tag{3.7}$$

$$a_k^+ - a_k^- = \mathrm{i}\sqrt{2}\sqrt{H}k\chi_k. \tag{3.8}$$

Here Q is the linear PV (2.3), and $V = f\Psi - gh$ is a measure of geostrophic imbalance. The quantity $\nabla^2 V$ has been called by several names in the literature, including: imbalance (Vallis 1996), geostrophic departure (Warn *et al.* 1995) and a geostrophic vorticity (Mohebalhojeh & Dritschel 2001). For $k = 0$, the relation is

$$\begin{pmatrix} \sqrt{H}u_0 \\ \sqrt{H}v_0 \\ \sqrt{g}h_0 \end{pmatrix} = a^0(\boldsymbol{0}, t)\boldsymbol{\phi}_0^0 + a^+(\boldsymbol{0}, t)\boldsymbol{\phi}_0^+ + a^-(\boldsymbol{0}, t)\boldsymbol{\phi}_0^-, \tag{3.9}$$

from which

$$a_0^0 = \sqrt{g}h_0, \tag{3.10}$$

$$a_0^+ + a_0^- = \sqrt{2}\sqrt{H}v_0, \tag{3.11}$$

$$a_0^+ - a_0^- = -\mathrm{i}\sqrt{2}\sqrt{H}u_0. \tag{3.12}$$

It is convenient to present the models by defining

$$A \equiv (f^2 - c^2\nabla^2)^{-1}c^2Q \qquad \text{and} \qquad B \equiv (f^2 - c^2\nabla^2)^{-1}V, \tag{3.13}$$

and note by (3.6), A is derived from the vortical modes and by (3.7), B is derived from the IG modes.

3.2.1. *PPG (Vortical–Vortical–IG mode interactions added to QG)*

In addition to all the interactions among the vortical modes, the PPG model extends QG by adding all interactions including exactly one IG mode. Symbolically, the PPG

model is written as

$$\frac{\partial a_k^0}{\partial t} = 00 \oplus 0 + \oplus 0 - \tag{3.14}$$

$$\frac{\partial a_k^+}{\partial t} + i\omega_k a_k^+ = 00 \tag{3.15}$$

$$\frac{\partial a_k^-}{\partial t} - i\omega_k a_k^- = 00 \tag{3.16}$$

where the symbol $\oplus$ is used to mean 'also including' in this paper. The physical space PPG model results from an inverse transform of (3.14)–(3.16). To obtain results in terms of the variables Q, V and χ, add (3.15) and (3.16), and subtract (3.16) from (3.15). The results are

$$\frac{\partial a_k^0}{\partial t} = \sum_{\triangle} \frac{\overline{a_p^0}}{\omega_p \omega_q \omega_k} \left\{ \frac{\overline{a_q^0}}{\sqrt{H}} c(\boldsymbol{p} \times \boldsymbol{q} \cdot \hat{\boldsymbol{z}}) \left(\frac{\omega_q^2 - \omega_p^2}{2} \right) + \frac{\overline{(a_q^+ + a_q^-)}}{\sqrt{2q}\sqrt{H}} f(\boldsymbol{p} \times \boldsymbol{q} \cdot \hat{\boldsymbol{z}})\omega_p^2 \right.$$
$$\left. + \frac{\overline{(a_q^+ - a_q^-)}}{\sqrt{2q}\sqrt{H}} i\omega_q \omega_p^2 (\boldsymbol{p} \cdot \boldsymbol{q} + q^2) \right\} + \frac{a_k^0}{\sqrt{2}\sqrt{H}}(a_0^+(k_x - ik_y) + a_0^-(-k_x - ik_y)), \tag{3.17}$$

$$\frac{\partial(a_k^+ + a_k^-)}{\partial t} + i\omega_k(a_k^+ - a_k^-) = \frac{1}{\sqrt{H}} \sum_{k+p+q=0} \frac{\overline{a_p^0 a_q^0}}{\sqrt{2\omega_p \omega_q \omega_k}k} f(\boldsymbol{p} \times \boldsymbol{q} \cdot \hat{\boldsymbol{z}})(\omega_p^2 - \omega_q^2), \tag{3.18}$$

$$\frac{\partial(a_k^+ - a_k^-)}{\partial t} + i\omega_k(a_k^+ + a_k^-) = \frac{1}{\sqrt{H}} \sum_{k+p+q=0} -2i \frac{\overline{a_p^0 a_q^0}}{\sqrt{2\omega_p \omega_q \omega_k}k} \omega_k c^2(\boldsymbol{p} \times \boldsymbol{q} \cdot \hat{\boldsymbol{z}})^2, \tag{3.19}$$

where $\triangle$ represents $\boldsymbol{k} + \boldsymbol{p} + \boldsymbol{q} = 0$ for non-zero $\boldsymbol{k}$, $\boldsymbol{p}$ and $\boldsymbol{q}$.

A sum over $\boldsymbol{k}$ of (3.17)–(3.19) and an inverse Fourier transform obtains

$$\frac{\partial Q}{\partial t} + J(\Psi, Q) + \nabla\chi \cdot \nabla Q + \langle u \rangle \frac{\partial Q}{\partial x} + \langle v \rangle \frac{\partial Q}{\partial y} + Q\nabla^2\chi = 0, \tag{3.20}$$

$$\frac{\partial \nabla^2 V}{\partial t} - c^2\nabla^4\chi + f^2\nabla^2\chi = f J(A, Q), \tag{3.21}$$

$$\frac{\partial \nabla^2 \chi}{\partial t} - \nabla^2 V = 2J\left(\frac{\partial A}{\partial x}, \frac{\partial A}{\partial y} \right), \tag{3.22}$$

where definitions (3.13) have been used.

Some discussion about the right-hand sides of (3.21) and (3.22) is warranted. From the definitions of Q and V and (3.13) it is found that

$$\Psi = (f^2 - c^2\nabla^2)^{-1}(fV - c^2Q) = fB - A,$$
$$h = (f^2 - c^2\nabla^2)^{-1}(H\nabla^2 V - fHQ) = H\nabla^2 B - \frac{f}{g}A. \tag{3.23}$$

Since PPG includes only interactions that have at least one vortical mode in the quadratic interaction and the vortical modes contain all the linear PV, some linear PV present is necessary for nonlinear coupling to occur. However, the nonlinear terms of (3.21) and (3.22) show how an unbalanced component of the flow can develop even for initial conditions in geostrophic balance ($f\Psi = gh$), for which $A = (f^2 - c^2\nabla^2)^{-1}c^2Q = -\Psi$. Then the nonlinear terms of (3.21) and (3.22) reduce to $-fJ(\Psi, Q)$ and $2J(\Psi_x, \Psi_y)$, respectively. In general, by the first relation of (3.23),

the nonlinear terms can equivalently be written with these terms, $-fJ(\Psi, Q)$ and $2J(\Psi_x, \Psi_y)$, and additional terms involving $B = (f^2 - c^2\nabla^2)^{-1}V$.

3.2.2. *P2G (Vortical–IG–IG mode interactions added to PPG)*

Further vortical–IG mode interactions may be included by adding to PPG all interactions involving exactly two IG modes. The P2G model results after inverse Fourier transform of the (symbolic) equations

$$\frac{\partial a_k^0}{\partial t} = 00 \oplus 0 + \oplus 0 - \oplus + + \oplus + - \oplus - - \tag{3.24}$$

$$\frac{\partial a_k^+}{\partial t} + \mathrm{i}\omega_k a_k^+ = 00 \oplus 0 + \oplus 0 - \tag{3.25}$$

$$\frac{\partial a_k^-}{\partial t} - \mathrm{i}\omega_k a_k^- = 00 \oplus 0 + \oplus 0 - . \tag{3.26}$$

Notice that the right-hand side of (3.24) includes all interactions that occur for the time derivative of the amplitude of a vortical mode. Furthermore, since $0|++, 0|+-$ and $0|--$ are identically zero (appendix A, see also Warn 1986; Embid & Majda 1996), an inverse transform of (3.24) leads to (3.20), the same as the corresponding equation for PPG. Another way to see that (3.20) is already complete is to start from (2.1), take the curl of the momentum equations, subtract f/H times the h equation and see that (3.20) is obtained.

The Fourier space P2G equations are found in appendix C. In physical space the P2G model is

$$\frac{\partial \nabla^2 V}{\partial t} - c^2\nabla^4\chi + f^2\nabla^2\chi = gJ(\nabla^2\Psi, h) + \nabla^2 J(A, V) - J(\nabla^2 A, V)$$
$$- f\nabla^2(\nabla \cdot (A\nabla\chi)) + f\nabla \cdot (\nabla\chi\nabla^2 A) \tag{3.27}$$

$$\frac{\partial \nabla^2\chi}{\partial t} - \nabla^2 V = -2(J(A_x, \Psi_y) + J(\Psi_x, A_y) + J(A_x, A_y))$$
$$- \nabla^2 J(\chi, A) + J(\chi, \nabla^2 A) \tag{3.28}$$

$$\frac{\partial \langle u \rangle}{\partial t} - f\langle v \rangle = \langle A_y\nabla^2\chi \rangle \tag{3.29}$$

$$\frac{\partial \langle v \rangle}{\partial t} + f\langle u \rangle = \langle -A_x\nabla^2\chi \rangle. \tag{3.30}$$

Recall $A \equiv (f^2 - c^2\nabla^2)^{-1}c^2 Q$. As for PPG, by (3.23), the nonlinear terms may be written with terms involving B instead.

3.2.3. *GGG (IG–IG–IG interactions)*

Here the equations GGG are derived by considering only IG mode interactions. Hence, GGG is a model to study IG mode interactions in isolation from vortical mode interactions, but the GGG model is not an intermediate model (which implies an improvement upon QG). Symbolically, consider

$$\frac{\partial a_k^0}{\partial t} = 0 \tag{3.31}$$

$$\frac{\partial a_k^+}{\partial t} + \mathrm{i}\omega_k a_k^+ = + + \oplus + - \oplus - - \tag{3.32}$$

$$\frac{\partial a_k^-}{\partial t} - \mathrm{i}\omega_k a_k^- = + + \oplus + - \oplus - - . \tag{3.33}$$

The GGG Fourier space equations are given in appendix C. In physical space they are

$$\frac{\partial Q}{\partial t} = 0, \tag{3.34}$$

$$\frac{\partial \nabla^2(V)}{\partial t} - c^2\nabla^4\chi + f^2\nabla^2\chi = -\langle u\rangle\frac{\partial \nabla^2 V}{\partial x} - \langle v\rangle\frac{\partial \nabla^2 V}{\partial y}$$
$$-f^2\nabla\cdot(\nabla\chi\nabla^2 B) - f\nabla^2 J(B, V) + fJ(\nabla^2 B, V) + \nabla^2(\nabla\cdot(c^2\nabla^2 B\nabla\chi)), \tag{3.35}$$

$$\frac{\partial \nabla^2\chi}{\partial t} - f\nabla^2\psi + g\nabla^2 h = -\langle u\rangle\frac{\partial \nabla^2\chi}{\partial x} - \langle v\rangle\frac{\partial \nabla^2\chi}{\partial y}$$
$$-\nabla^2\left(\frac{(\nabla\chi)^2}{2}\right) + 2f^2 J(B_x, B_y) - fJ(\chi, \nabla^2 B) + f\nabla^2 J(\chi, B), \tag{3.36}$$

$$\frac{\partial \langle u\rangle}{\partial t} - f\langle v\rangle = \langle -fB_y\nabla^2\chi\rangle, \tag{3.37}$$

$$\frac{\partial \langle v\rangle}{\partial t} + f\langle u\rangle = \langle fB_x\nabla^2\chi\rangle. \tag{3.38}$$

Recall $B \equiv (f^2 - c^2\nabla^2)^{-1}V$.

3.2.4. *QVD (all interactions)*

Of course, if all interactions are included, an inverse Fourier transform must recover the equivalent of the full RSW equations. The form attained is denoted as QVD consisting of evolution equations for the linear PV Q, the imbalance $\nabla^2 V$ and the horizontal divergence $\nabla^2\chi$. In addition to (3.20), the QVD equations are

$$\frac{\partial \nabla^2(V)}{\partial t} + (f^2 - c^2\nabla^2)\nabla^2\chi = -\langle u\rangle\frac{\partial \nabla^2 V}{\partial x} - \langle v\rangle\frac{\partial \nabla^2 V}{\partial y} - fJ(\Psi, \nabla^2\Psi)$$
$$-f\nabla\cdot(\nabla^2\Psi\nabla\chi) + g\nabla^2(J(\Psi, h)) + g\nabla^2(\nabla\cdot(h\nabla\chi)), \tag{3.39}$$

$$\frac{\partial \nabla^2\chi}{\partial t} - \nabla^2 V = -\langle u\rangle\frac{\partial \nabla^2\chi}{\partial x} - \langle v\rangle\frac{\partial \nabla^2\chi}{\partial y}$$
$$-\nabla^2\left(\frac{(\nabla\chi)^2}{2}\right) + 2J(\Psi_x, \Psi_y) - J(\chi, \nabla^2\Psi) + \nabla^2 J(\chi, \Psi), \tag{3.40}$$

$$\frac{\partial \langle u\rangle}{\partial t} - f\langle v\rangle = -\langle\Psi_y\nabla^2\chi\rangle, \tag{3.41}$$

$$\frac{\partial \langle v\rangle}{\partial t} + f\langle u\rangle = \langle\Psi_x\nabla^2\chi\rangle. \tag{3.42}$$

Equations (3.39) and (3.40) are similar to (8) and (6) of Vallis (1996) minus the beta-effect. The nonlinear terms of the full QVD form are also obtained if the nonlinear terms of P2G and GGG are added together.

3.3. *Alternate derivation*

Starting from the QVD formulation, the models can be derived in physical space without utilizing Fourier transforms. The key relations are (3.23): $\Psi = fB - A$ and $h = H\nabla^2 B - (f/g)A$. By (3.13), A is related to the vortical modes while B is related to the IG modes. Further, by (3.8) and (3.11) and (3.12), χ, $\langle u\rangle$ and $\langle v\rangle$ are also related to the IG modes. Therefore, the nonlinear terms of the QVD formulation, (3.20), (3.39)–(3.42) can be written in terms of Q, V, A, B, χ and the mean flows. Each nonlinear term in the QVD equations involves products with zero, one or two

factors corresponding to the IG modes. Then to obtain the PPG model, for example, keep the products with zero or one factor related to the IG modes in the equation for Q; keep products with zero factors related to the IG modes in the equations for the imbalance $\nabla^2 V$ and the horizontal divergence $\nabla^2 \chi$.

4. Numerical results

Although they do not offer a numerical savings to RSW, the PPG and P2G models can be used to study vortical–IG mode interactions, e.g. which interactions are primarily responsible for anticyclone dominance observed in RSW decay. For the numerical calculations, dissipation in the form of hyper-diffusion is added to all variables for each model. The hyper-diffusion operator has the generic form

$$(-1)^{p+1}\nu\nabla^{2p}, \tag{4.1}$$

where ν is the dissipation coefficient and $2p$ is the order of the hyper-diffusion. The coefficient ν was adjusted so that the results given by the UVH (2.1) and QVD ((3.20), (3.39)–(3.42)) forms of RSW agreed within a small error; this corresponded to the level of dissipation necessary to obtain monotonic decay of energy in all models. All of the numerics reported herein were done using fourth-order hyper-diffusion.

The models PPG, P2G and GGG share the linear structure of the QVD formulation of the full equations dictated by the eigenmodes (one equation for the linear vortical mode in terms of Q and two for the linear gravity wave modes in terms of $\nabla^2 V$ and $\nabla^2 \chi$). In order to numerically integrate the equations with this linear structure, the equivalent to (2.14) is used. Substituting a Fourier mode

$$\begin{pmatrix} Q \\ \nabla^2 V \\ \nabla^2 \chi \end{pmatrix}(\boldsymbol{x}, t) = \widehat{\begin{pmatrix} Q \\ \nabla^2 V \\ \nabla^2 \chi \end{pmatrix}}(\boldsymbol{k}, t)\mathrm{e}^{\mathrm{i}(\boldsymbol{k}\cdot\boldsymbol{x} - \omega(\boldsymbol{k})t)}, \tag{4.2}$$

into the linear part of the models does not give a skew-Hermitian system. However, by setting $\nabla^2 V(\boldsymbol{k}) = \omega_k Z(\boldsymbol{k})$, a factor of ω_k can be pulled out of the equation for $\nabla^2 V$. With ω_k factored out, a skew-Hermitian matrix that multiplies $(Q(\boldsymbol{k}), Z(\boldsymbol{k}), \nabla^2\chi(\boldsymbol{k}))^{\mathrm{T}}$ is obtained. This matrix has the eigenfunctions

$$\boldsymbol{\varphi}^0 = \begin{pmatrix} 1 \\ 0 \\ 0 \end{pmatrix}, \quad \boldsymbol{\varphi}^+ = \frac{1}{2}\begin{pmatrix} 0 \\ 1 - \mathrm{i} \\ 1 + \mathrm{i} \end{pmatrix}, \quad \boldsymbol{\varphi}^- = \frac{1}{2}\begin{pmatrix} 0 \\ 1 + \mathrm{i} \\ 1 - \mathrm{i} \end{pmatrix}. \tag{4.3}$$

Hence,

$$\begin{pmatrix} Q \\ \nabla^2 V \\ \nabla^2 \chi \end{pmatrix}(\boldsymbol{x}, t) = \sum_{\boldsymbol{k}} \begin{pmatrix} 1 & 0 & 0 \\ 0 & \omega_k & 0 \\ 0 & 0 & 1 \end{pmatrix}\begin{pmatrix} Q \\ Z \\ \nabla^2 \chi \end{pmatrix}(\boldsymbol{k}, t)\mathrm{e}^{\mathrm{i}\boldsymbol{k}\cdot\boldsymbol{x}}, \tag{4.4}$$

where

$$\begin{pmatrix} Q \\ Z \\ \nabla^2 \chi \end{pmatrix}(\boldsymbol{k}, t) = (b^0(\boldsymbol{k}, t)\boldsymbol{\varphi}^0 + b^+(\boldsymbol{k}, t)\boldsymbol{\varphi}^+ + b^-(\boldsymbol{k}, t)\boldsymbol{\varphi}^-); \tag{4.5}$$

see also Mohebalhojeh & Dritschel (2001).

Thereby, a Fourier transform of any model with the QVD linear form leads to

$$\frac{\partial b_k^0}{\partial t}\boldsymbol{\varphi}_k^0 + \frac{\partial b_k^+}{\partial t}\boldsymbol{\varphi}_k^+ + \frac{\partial b_k^-}{\partial t}\boldsymbol{\varphi}_k^- + i\omega_k^0 b_k^0 \boldsymbol{\varphi}_k^0 + i\omega_k^+ b_k^+ \boldsymbol{\varphi}_k^+ + i\omega_k^- b_k^- \boldsymbol{\varphi}_k^-$$

$$+\nu k^{2p} b_k^0 \boldsymbol{\varphi}_k^0 + \nu k^{2p} b_k^+ \boldsymbol{\varphi}_k^+ + \nu k^{2p} b_k^- \boldsymbol{\varphi}_k^- = \begin{pmatrix} 1 & 0 & 0 \\ 0 & \frac{1}{\omega_k} & 0 \\ 0 & 0 & 1 \end{pmatrix} \widehat{NL}_k, \qquad (4.6)$$

where $\widehat{NL}_k$ is the $\boldsymbol{k}$ component of the nonlinear term of the particular model. The orthonormal property of the eigenfunctions is used to divide (4.6) into three equations, one for each amplitude b_k^0, b_k^+ and b_k^-. We treat the linear part, dispersive and diffusive terms, with an integrating factor and advance in time using a standard RK3 scheme. All equations use a pseudo-spectral scheme for the spatial discretization. All nonlinear calculations are dealiased by padding via the 3/2 rule and done at 384^2 (leaving a true resolution of 256^2). The time step was determined by the minimum of the value given by the CFL condition times a safety factor, and the value so that there are 10 data points per period of the wave with the largest frequency. The latter was the more restrictive.

4.1. *Initial conditions*

We consider numerical decay from two sets of initial conditions for a range of Rossby Ro and Froude Fr numbers, $0.25 \leqslant Ro = U/(fL) \leqslant 1$ and $0.1 \leqslant Fr = U/(gH) \leqslant 0.3$. Here U is the initial root mean square velocity and L is a length scale characterizing the initial structures (their values and an explanation is forthcoming). We use the procedure described in Polvani *et al.* (1994) to initialize the streamfunction Ψ for both sets of initial conditions. The initial magnitude of Ψ_k is determined by

$$| \Psi_k |^2 \propto \frac{k^{12.5}}{(k + 14)^{25}k^2}, \qquad (4.7)$$

where k is the magnitude of the non-dimensional wavevector (non-dimensionalized by $2\pi/L_D$ where L_D is the dimension of the periodic box). Then the phase of each Ψ_k is chosen from a uniform $(0,2\pi)$ distribution. For one set of initial conditions, group B, we initialize h and χ by inverting the dimensional form of Polvani *et al.* (1994) equations (2.5a–c), which are as follows (see Polvani *et al.* 1994, for more details):

$$\nabla^2 \Psi_t = -\nabla \cdot (\nabla^2 \Psi \nabla \chi) - J(\Psi, \nabla^2 \Psi) - f\nabla^2 \chi, \qquad (4.8)$$

$$g\nabla^2 h = f\nabla^2 \Psi + 2J(\Psi_x, \Psi_y), \qquad (4.9)$$

$$\left(\nabla^2 - \frac{f^2}{gH}\right)\nabla^2 \chi = \frac{f}{gH}\nabla \cdot (\nabla^2 \Psi \nabla \chi) + \frac{f}{gH}J(\Psi, \nabla^2 \Psi)$$

$$- \frac{2}{gH}J(\Psi_x, \Psi_y)_t - \frac{1}{H}\nabla^2(\nabla \cdot h\nabla \chi) - \frac{1}{H}\nabla^2 J(\Psi, h). \qquad (4.10)$$

This set will be referred to as balanced initial conditions.

For the second set of initial conditions, group A and referred to as unbalanced, the height perturbation h is given the initial value zero. Group A is further categorized by the percentage, X, of the total initial energy that is divergence free. To achieve this, the initial magnitudes of Ψ_k and χ_k are determined by

$$| \Psi_k |^2 = CX\frac{k^{12.5}}{(k + 14)^{25}k^2} \quad \text{and} \quad | \chi_k |^2 = C(1 - X)\frac{k^{12.5}}{(k + 14)^{25}k^2}, \qquad (4.11)$$

where C is a constant of proportionality. The phase of each Ψ_k and χ_k is chosen from a uniform $(0, 2\pi)$ distribution. To distinguish the runs A, the percentage of initial energy that is divergence free is part of the label as in AX (e.g. A100).

To set up the numerics, Yuan & Hamilton (1994) was followed and geophysically relevant parameters were used instead of using a 2π periodic box and dimensionless numbers. The domain size for all numerics is $L_D = 4\pi \times 10^6$ m. Since (4.7) gives a (non-dimensional) centroid wavenumber of 18, a consistent length scale is $L = 1.4 \times 10^5$ m. For every run the initial root mean square velocity is $U_{rms} = 10$ m s^{-1}, which is easily attained by adjusting the proportionality constant in (4.7) or (4.11). Therefore, the eddy turn over time, $L/U = 1.4 \times 10^4$ s. Note that Ro and Fr can be set to desired values by appropriately picking f and H, respectively. A range of Ro and Fr were chosen that cover a subset of that covered by Polvani *et al.* (1994) (they explored much larger Ro values).

For all plots spatial dimensions are reported in terms of the length scale L, time and vorticity dimensions are reported in terms of eddy turn over times L/U and energy is non-dimensionalized by $H U_{rms}^2 L_D^2 / 2$. Plots pertaining to a specific time correspond to data obtained at 500 turnover times.

4.2. *Results*

4.2.1. *Energy*

As discussed, two difficulties occur with the non-quadratic invariants. The first difficulty that arises from the necessary truncation in wavenumber is the possibility of leakage of an invariant into or out of the reduced system (Warn 1986). Second is (and related to the first), since individual triads cannot be shown to conserve the non-quadratic invariants, we could not show that the reduced models conserve analogues of these non-quadratic invariants (other than QG). Therefore, it is important to monitor the energy in the models and make sure that it behaves reasonably. Figure 1 shows a representative plot of energy versus time for the unbalanced (A100) and balanced initial conditions. In both cases, the behaviour of the energy in the models PPG and P2G qualitatively and quantitatively resembles that of the energy in RSW; furthermore, the energy monotonically decays in time. However, with the A100 initial conditions distinctions occur among the three models. In particular, the rate of energy decay is consistent with the number of subsets of interactions involving IG modes contained by each model. We also refer the reader ahead to figure 18 showing energy versus time for more unbalanced initial conditions A25, A5 and A0. Notice that the rate of energy decay in RSW increases with the level of divergence in the initial conditions. In addition, the difference between the decay rate for RSW and the decay rates for PPG/P2G increases with larger initial divergence. The latter result is sensible since RSW contains the most gravity wave activity. The reason that the energy decay for PPG and P2G is identical for A0 initial conditions will become evident in §5.

4.2.2. *Fields of vorticity*

Contour plots of the fields of vorticity for the different models are found in figure 2 for initial conditions A100 and in figure 3 for balanced initial conditions. All plots correspond to data obtained at 500 turnover times and the same parameters ($Ro = .25$ and $Fr = .2$). Notice in figure 2 the difference between the QG model and all other models. It is apparent that when the interactions involving one IG mode and two vortical modes are retained along with the interactions among three vortical modes, anticyclones dominate for these parameters ($Ro = .25$ and $Fr = .2$). Also notice the smaller scales present when there are interactions among IG modes. Moreover, the
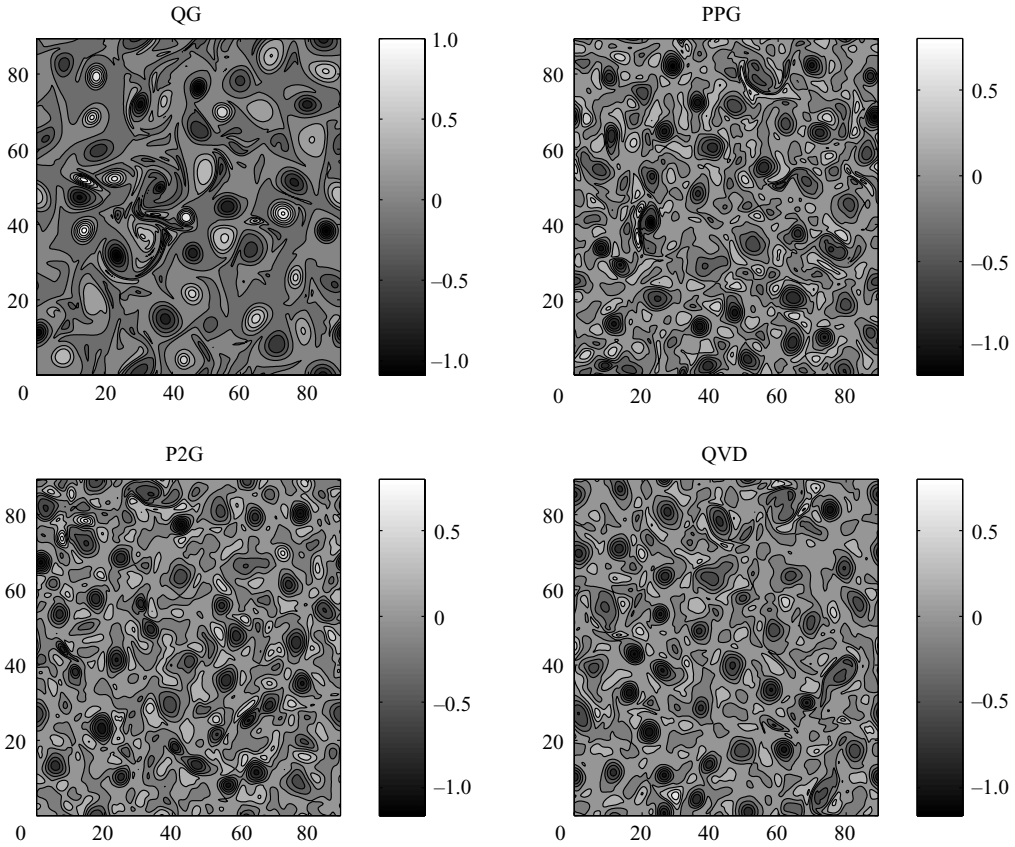
FIGURE 2. Vorticity: $Ro = .25$ and $Fr = .2$. Unbalanced initial conditions.

size of the structures depends on the initial conditions. When the initial conditions are unbalanced, smaller structures are attained. This is attributed to increased gravity wave activity due to a larger initial projection onto the IG modes. In figure 3, QVD and UVH correspond to the full equations integrated in the different forms. The similarity between these two fields is a visual check on the numerical procedures and level of diffusivity.

4.2.3. *Size of vortices*

As a measure of the size of the vortices, the centroid may be defined as

$$\text{Cent}(k) = \frac{\left(\sum_{k} k (|u_k|^2 + |v_k|^2) \right)}{\sum_{k} (|u_k|^2 + |v_k|^2)}. \tag{4.12}$$

The minimum value of the centroid attained for a run is found in tables 1 and 2 for balanced and A100 initial conditions, respectively. In addition, representative plots of the centroid as a function of time are reported in figure 4 for A100 initial conditions and in figure 5 for balanced initial conditions. The initial value of the centroid is 18. As in Polvani *et al.* (1994) we find that smaller centroid values (larger coherent structures) are associated with larger Burger number for RSW. A discussion on this association is found there including plots and energy considerations as the structures
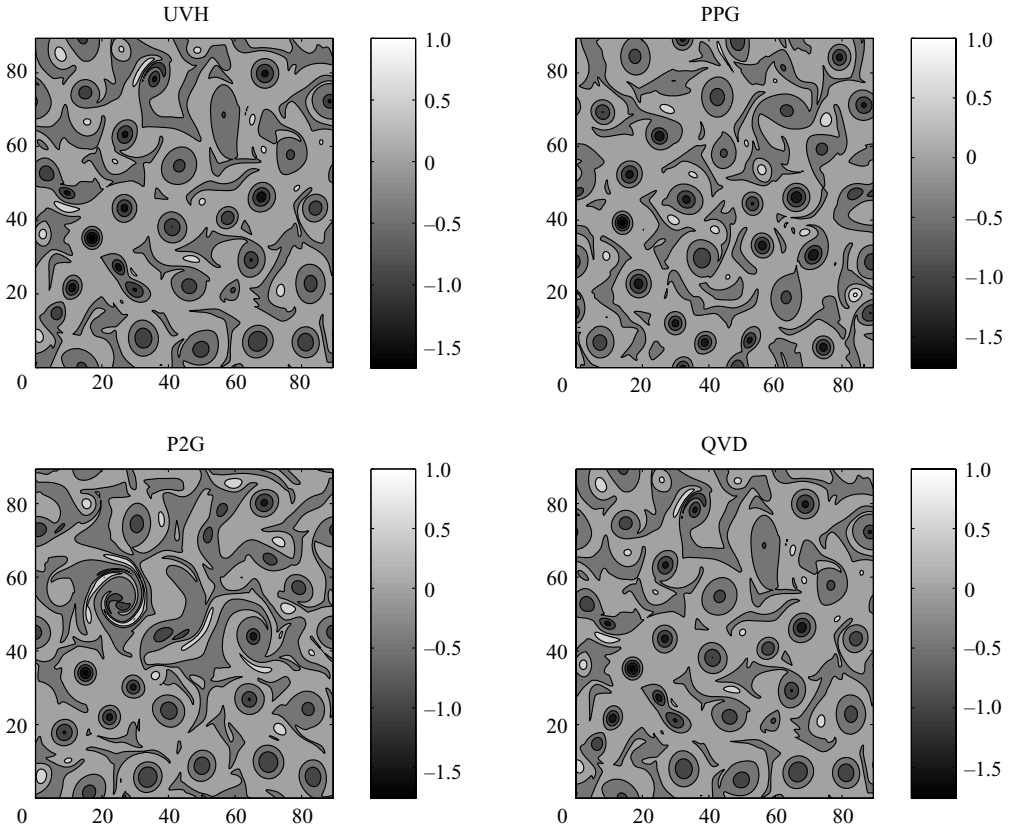
FIGURE 3. Vorticity: $Ro = .25$ and $Fr = .2$. Balanced initial conditions.

grow. The Burger number (Bu) is

$$Bu = \left(\frac{Ro}{Fr}\right)^2 = \left(\frac{L_R}{L}\right)^2, \tag{4.13}$$

where $L_R = \sqrt{gH}/f$ is the Rossby radius of deformation. Hence, the smaller the initial vortex size compared to the Rossby radius of deformation, the smaller the centroid values attained. In fact, for the balanced initial conditions, the initial Bu of a run consistently predicts where its resulting centroid will fall with respect to the other runs tested (see table 1). For unbalanced initial conditions, the initial Bu continues to be an excellent indicator, with only run s out of order (see table 2). In figure 4 we see that the QG model allows the vortices to grow the largest in size. Both figures 4 and 5 show that the models containing the interactions between two vortical modes and one IG mode along with the interactions among the vortical modes lead to similar growth in time of the size of the vortices for balanced and unbalanced divergence free initial conditions. These results indicate that, whether the inertial-gravity waves tend to break up coherent structures or, alternatively, that they adversely effect the merger of like signed vortices, the mode interactions with exactly one IG wave mode are largely responsible for the inertial-gravity wave activity in RSW for these initial conditions. Of course, that waves can diminish coherent structures has been noted

Run	Fr	Ro	Bu	Model	Min. skewness	Max. kurtosis	Min. centroid
ne	.1	.25	6.25	RSW	−2.0869	15.5542	3.8551
n	.1	.4	16	RSW	−1.9786	18.3945	3.1184
				PPG	−2.3025	18.2871	3.2190
				P2G	−2.3122	19.6314	2.9176
ng	.1	1	100	RSW	−1.6142	30.0610	2.1251
e	.2	.25	1.5625	RSW	−1.9439	8.1524	5.4406
				PPG	−1.9754	8.7626	5.4999
				P2G	−1.9819	8.9138	5.2668
en	.2	.4	4	RSW	−2.5001	12.2113	4.7425
q	.25	.4	2.560	RSW	−2.4122	10.6519	5.3361
				PPG	−2.5367	11.6692	5.4863
				P2G	−2.2617	10.1176	5.2127
g	.3	1	11.1111	RSW	−3.6675	21.4015	3.7383
				PPG	−3.6742	20.0154	4.3410
				P2G	−3.5242	18.8147	3.9625

TABLE 1. Balanced initial data (group B).

Run	Fr	Ro	Bu	Model	Min. skewness	Max. kurtosis	Min. centroid
n	.1	.4	16	RSW	−2.3469	17.0606	3.1940
				PPG	−2.9495	20.2775	3.2863
				P2G	−2.4513	16.3508	3.2314
e	.2	.25	1.5625	RSW	−1.2562	5.8498	6.6990
				PPG	−1.2005	5.5342	7.0476
				P2G	−1.1664	5.4537	6.9269
q	.25	.4	2.560	RSW	−2.2339	8.7629	6.5357
				PPG	−2.0079	8.2410	6.5631
				P2G	−1.9044	7.5554	6.4945
s	.3	.4	1.7778	RSW	−1.7473	7.3709	7.0366
				PPG	−1.5492	6.3412	7.3657
				P2G	−1.5268	6.3984	7.2340
g	.3	1	11.1111	RSW	−3.3640	15.6876	4.6613
				PPG	−3.2899	15.0733	4.8978
				P2G	−3.2848	14.8449	4.8412

TABLE 2. Unbalanced 100 % divergence free initial data (group A100).

before, for example, Maltrud & Vallis (1990) found that excitation of Rossby waves had this effect on coherent structures in the barotropic β-plane model.

The kurtosis of vorticity is positively correlated with the size of the coherent structures and measures the intermittency of the flow (Mcwilliams 1984, page 25)

$$\text{Kurt}(\nabla^2 \Psi) = \frac{\int_A (\nabla^2 \Psi)^4 \, dA}{\left(\int_A (\nabla^2 \Psi)^2 \, dA\right)^2}. \tag{4.14}$$

Again, as in Polvani *et al.* (1994), the Burger number is the non-dimensional number that predicts where the value of the kurtosis of a run will fall compared to other runs. The larger the Burger number, the more intermittent (greater kurtosis) the field is expected to become. For balanced initial conditions only the values of kurtosis for runs *g* and *n* are not in line with their Burger number (table 1). Note that these two runs have similar Burger numbers, but there is a large difference in their *Fr* numbers. The kurtosis for all the runs with A100 initial data are in order with their
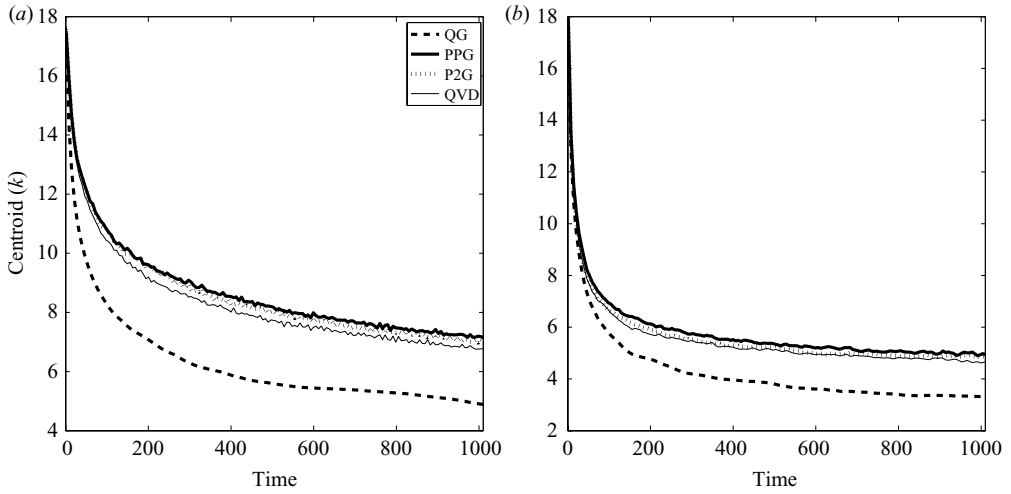
FIGURE 4. Centroid versus time. Unbalanced initial conditions, A100. (*a*) $Ro = .25$ and $Fr = .2$. (*b*) $Ro = 1$ and $Fr = .3$.
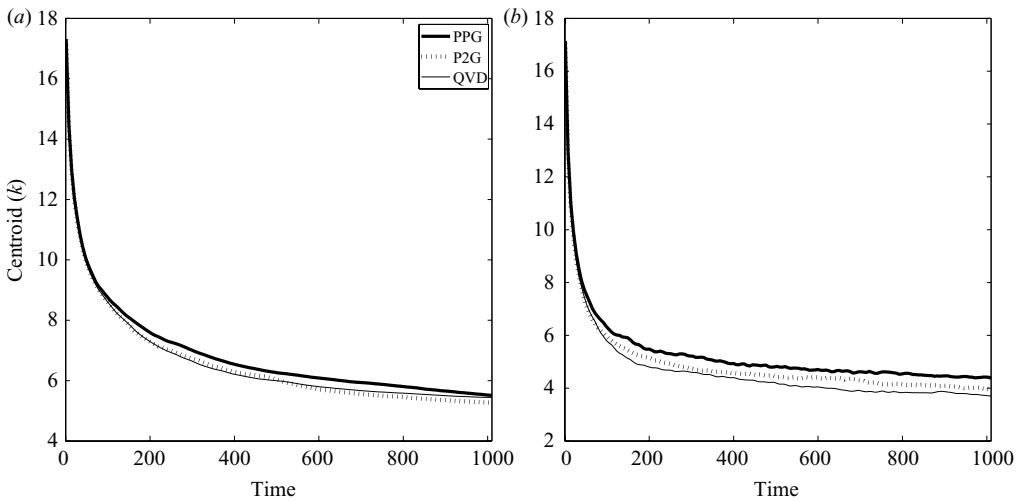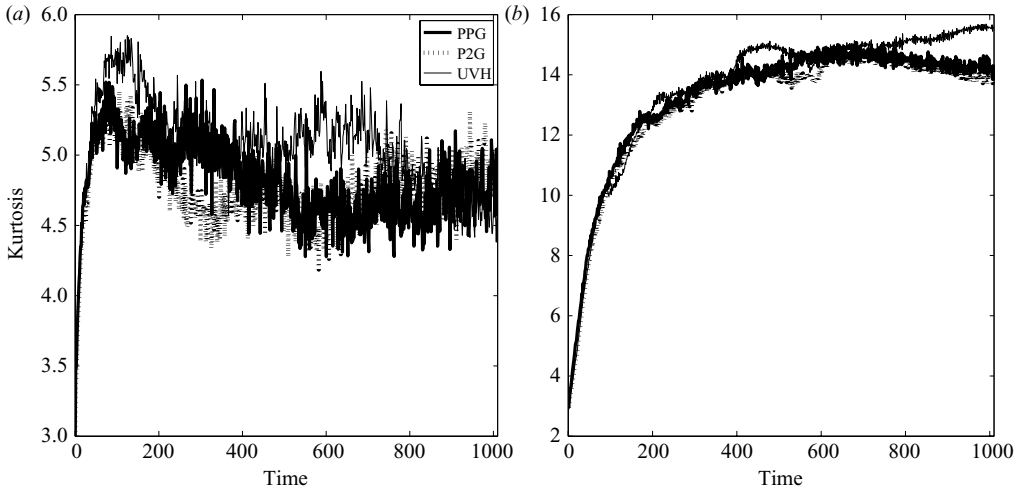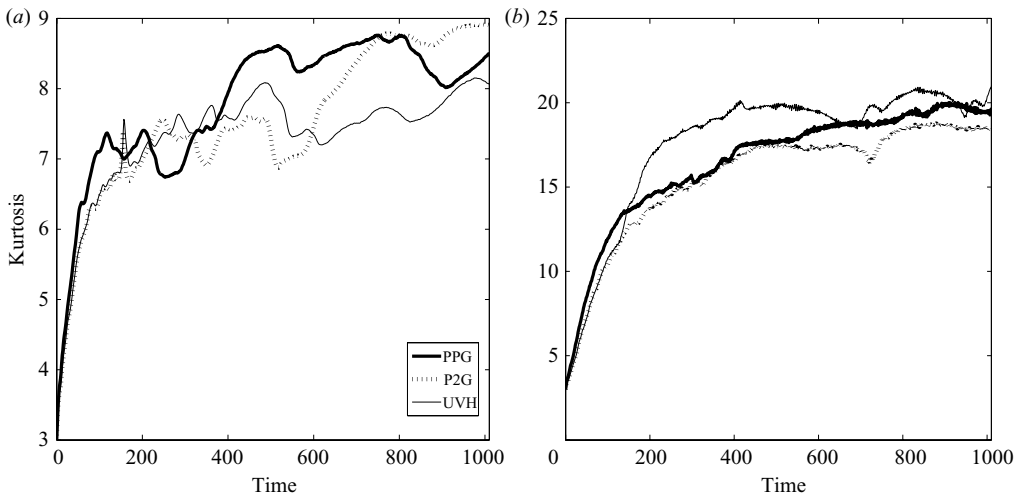

FIGURE 5. Centroid versus time. Balanced initial conditions. (*a*) $Ro = .25$ and $Fr = .2$. (*b*) $Ro = 1$ and $Fr = .3$.

Burger numbers (table 2). For these two sets of initial data PPG, P2G and RSW have comparable levels of intermittency in time (for representative plots see figure 6 for A100 and figure 7 for balanced initial conditions).

4.3. *Cyclone anticyclone asymmetry*

The skewness of the vorticity

$$\mathrm{Skew}(\nabla^2 \Psi) = \frac{\int_A (\nabla^2 \Psi)^3 \, \mathrm{d}A}{\left(\int_A (\nabla^2 \Psi)^2 \, \mathrm{d}A \right)^{3/2}}, \qquad (4.15)$$

as a function of time and the p.d.f. of the vorticity at 500 turnover times may be used to quantify the asymmetry between cyclones and anticyclones. Plots for two of the

FIGURE 6. Kurtosis versus time. Unbalanced initial conditions, A100. (*a*) $Ro = .25$ and $Fr = .2$. (*b*) $Ro = 1$ and $Fr = .3$.

FIGURE 7. Kurtosis versus time. Balanced initial conditions. (*a*) $Ro = .25$ and $Fr = .2$. (*b*) $Ro = 1$ and $Fr = .3$.

runs with A100 initial conditions are found in figures 8 and 9 and two for those with balanced initial conditions are in figures 10 and 11. In addition, the largest negative value of skewness attained is recorded in tables 1 and 2 for runs with balanced and A100 initial conditions, respectively. For all runs, the value of the skewness given by the initial conditions is near zero but slightly positive, with a value of 0.0066. When the linearized equations are integrated, the parity between cyclones and anticyclones is maintained. Reversing the direction of rotation of the rotating frame (a change in the sign of f) in RSW leads to a positive skewness of roughly the same magnitude, also a preference for anticyclones (both preceding results are excluded from the figures for clarity). For the parameter regime shown, a preference for anticyclones develops when the mode interactions involving at least one IG mode are included beyond QG (PPG, P2G and QVD). As found in Polvani *et al.* (1994) anticyclone dominance tends
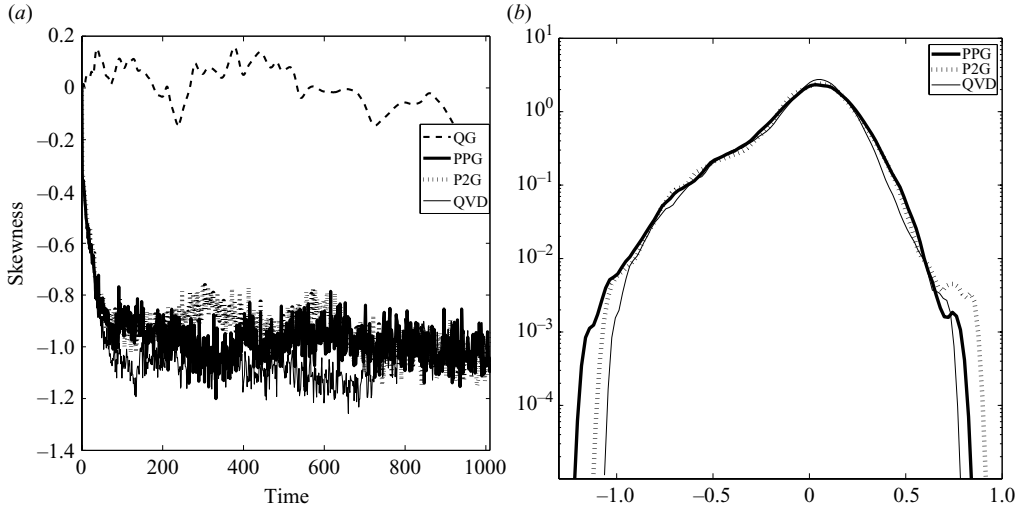
FIGURE 8. $Ro = .25$ and $Fr = .2$. Unbalanced initial conditions, A100. (*a*) Skewness versus time. (*b*) Asymmetric p.d.f.'s.
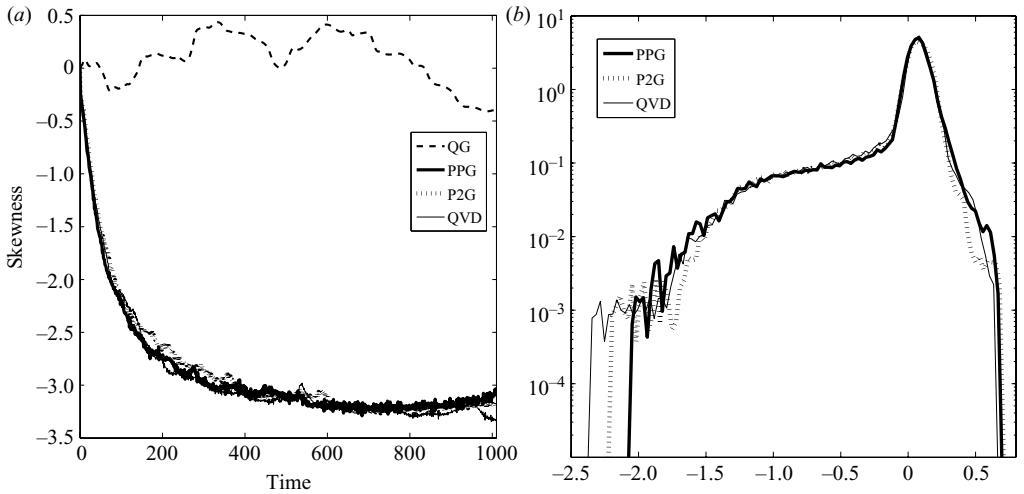

FIGURE 9. $Ro = 1$ and $Fr = .3$. Unbalanced initial conditions, A100. (*a*) Skewness versus time. (*b*) p.d.f. at 7.2×10^6 s about 500 turnover times.

to increase with increasing Fr. Furthermore, PPG, P2G and QVD have roughly the same behaviour in the skewness versus time and shape for the p.d.f.'s of vorticity for the balanced and A100 initial conditions at each set of Ro and Fr tested, indicating a relatively unimportant role of mode interactions containing exactly two IG modes and those containing three IG modes compared to those containing exactly one IG mode in the preference for anticyclones in RSW (the interactions among three IG modes do have a role in the asymmetry for certain initial conditions, see §5). For insight into the roles of these classes of interactions in the context of RBE, see the theoretical work by Babin, Mahalov & Nicolaenko (2002) and the combined theoretical/numerical discussions in Waite & Bartello (2006) and Sukhatme & Smith (2008). The exclusion of all interactions involving an IG mode (QG dynamics) results
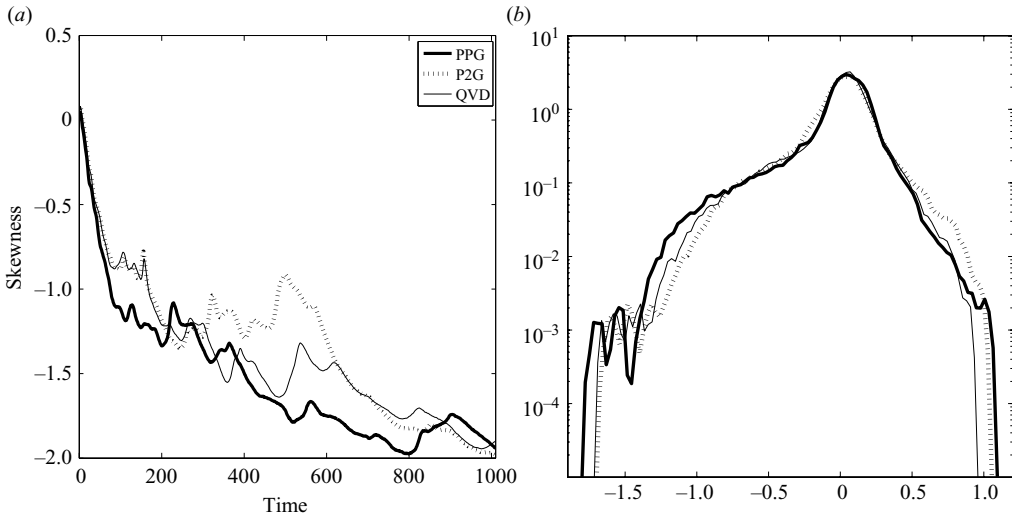
FIGURE 10. $Ro = .25$ and $Fr = .2$. Balanced initial conditions. (*a*) Skewness versus time.
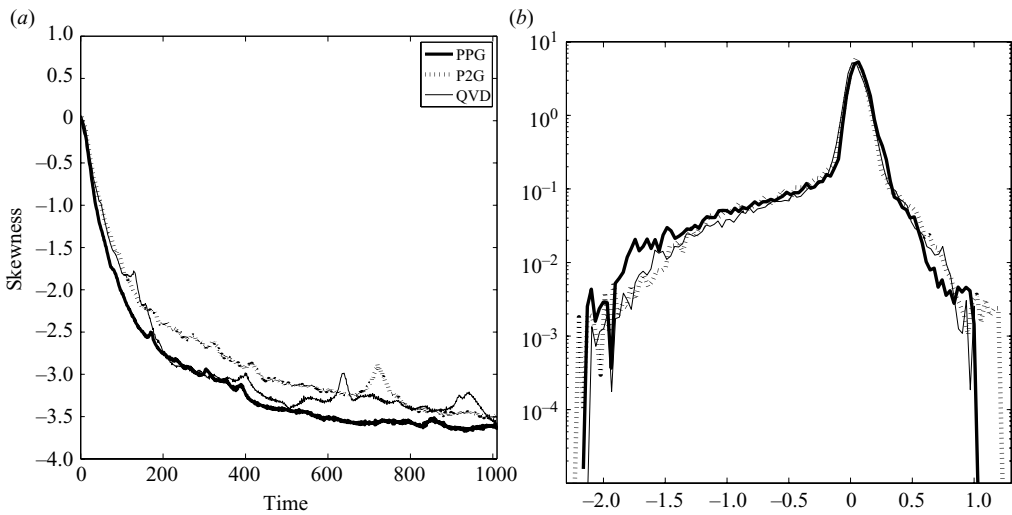(*b*) p.d.f. at 7.2×10^6 s about 500 turnover times.

FIGURE 11. $Ro = 1$ and $Fr = .3$. Balanced initial conditions. (*a*) Skewness versus time.
(*b*) p.d.f. at 7.2×10^6 s about 500 turnover times.

in p.d.f.'s that are symmetric and skewness values that hover around zero as expected (see also Polvani *et al.* 1994; Kuo & Polvani 2000).

Considering the balanced initial conditions, one can see that there is more influencing the final level of skewness than just the initial Fr. The initial size of the structures, and therefore the initial Bu, also plays a role in predicting the resulting level of skewness. For instance, runs n and e attain comparable values of the skewness. In fact, run e with twice the initial Fr attains a less negative minimum value of skewness than run n. However, run n has a larger initial Bu, larger structures and a more intermittent field (see table 1).
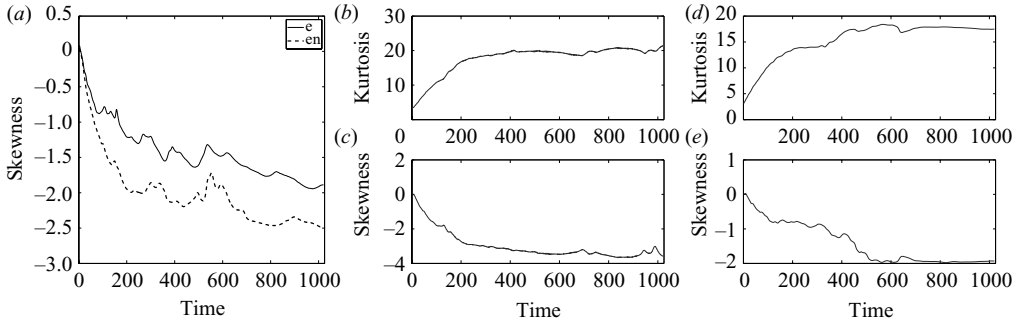
FIGURE 12. (*a*) Skewness versus time for A100 initial conditions at $Fr = .2$. The more skewed plot has a larger Burger number. (*b* and *c*) Relationship between intermittency and skewness, run *g*. (*d* and *e*) Relationship between intermittency and skewness at low Fr, run *n*. In general, an increase (decrease) in the intermittency corresponds to an increase (decrease) in the magnitude of skewness.

At larger initial $Fr \geqslant .2$, in general the skewness in the vorticity field increases with the initial Bu. For example, one may compare run *en* with run *e*. Both runs have the same initial Fr, but run *en* has a larger initial Bu. The skewness value for run *en* is always below the skewness value of run *e*, and the difference is severe (left plot figure 12). A large initial Fr along with a large initial Bu leads to a very skewed field (run *g*, table 1). Interestingly, the opposite trend is observed at low $Fr = .1$: a smaller initial Bu leads to a more skewed vorticity field among the three runs tested at this Fr (table 1).

For a particular run, regardless of initial Fr, an increase in intermittency as measured by the kurtosis generally corresponds to an increase in anticyclone dominance as measured by the skewness. Figure 12(*b–e*) shows this mirror relationship between the kurtosis and skewness for a run with a high and a low Fr, respectively. This indicates that the negative values of vorticity dominate as more weight is placed on extreme values of vorticity.

For A100 initial conditions, it is also found that the Fr is an incomplete predictor of the resulting asymmetry in the vorticity field and that the Bu again plays a role. In fact, for $Fr \geqslant .2$ the Bu predicts the resulting level of asymmetry for a run, with the level of dominance of the anticyclones increasing with initial Bu (table 2).

4.4. *Discussion*

It is apparent that, besides limiting the growth of coherent structures, interactions involving IG modes play an important role in the dominance of anticyclones. When the QG equation is integrated, the p.d.f. of vorticity is quite symmetric and the skewness remains close to zero as expected (Polvani *et al.* 1994; Kuo & Polvani 2000). The addition of interactions involving exactly one IG mode leads to a drastic change. The p.d.f. is far from symmetric and the skewness attains negative values for the parameter range reported. These effects are amplified, in general, with increasing Fr number as in Polvani *et al.* (1994).

Since A100 initial conditions project stronger onto the IG modes than balanced initial conditions, the results obtained from the two sets can provide more insight into the role of interactions. For example, starting from A100 initial conditions, RSW in general yields the most negative values of skewness, followed by PPG, then P2G (table 2). On the other hand, starting from balanced initial conditions, in general PPG

yields the largest negative values (table 1). Note an exception is for the low *Fr* run, run *n*, for this run the skewness of PPG is the most negative for virtually the entire duration of the run for both initial conditions (plots excluded). These observations suggest that with even more imbalance in the initial conditions, RSW will show greater negative values of the skewness than PPG and P2G, at least for runs with larger *Fr*. This will be confirmed when divergence is added to the initial conditions, shedding light on the role of the GGG interactions (see § 5).

Differences observed between PPG and P2G would help determine the role of the interactions $\pm|0\pm$, all of which are catalytic (Warn 1986) in the sense that the slow mode is not changed in the interaction and there is transfer between the fast modes. Further, the interactions $+|0-$ and $-|0+$ are resonant catalytic if both wavenumber magnitudes of the fast modes belong to the same shell (i.e. have the same magnitude, Embid & Majda 1996). However, the role of these interactions is not elucidated by the statistics measured here; PPG captures the behaviour of RSW for the initial conditions considered, and there is little difference between PPG and P2G in the values of the measured statistics. It should be noted that RBE resonant catalytic interactions are likely to be more important than RSW resonant catalytic interactions, since RBE resonant catalytic interactions involve fast wavevectors on the same cone, thereby allowing transfer between scales. For RBE the resonant catalytic interactions have been shown to play a role in the transfer of energy towards smaller scales (Bartello 1995).

It is emphasized that there were no major differences between PPG and P2G for the statistics measured here. This does not mean that there are no differences in the evolution of a flow between PPG and P2G. For example, the detailed space–time evolution of the vortices may be influenced by the catalytic resonant interactions of RSW (absent in PPG but contained in P2G) which transfer energy between wavevectors of different orientation but not of different magnitude.

Further reduced models can be developed and tested. Two of these models are explicitly written in appendix D. One of these models, labelled P2SG, includes all the interactions of P2G less the interactions involving exactly one IG mode. The P2SG model displays no preference for anticyclones for A100 conditions. This result further shows the importance of the interactions involving one IG mode and two vortical modes in the preference for anticyclones in RSW, and is not surprising based on the similar results obtained for PPG and P2G. The P2SG model actually displays a slight bias for cyclones starting from balanced initial conditions, perhaps reflecting the slightly more skewed results of PPG than P2G for the same initial conditions (figures 10 and 11). The other of these models, labelled PPSG, excludes the interactions among the vortical modes from the PPG model and hence includes only the interactions with exactly one IG mode. The mimicking of the anticyclonic dominance of RSW found in PPG is absent from the PPSG model, showing that the presence of the interactions among the vortical modes plays a role in the asymmetry. However, energy considerations and structure size are factors when the interactions among the vortical modes are absent since, not surprisingly, energy dissipates faster and larger structures are inhibited (figures 13 and 14).

5. GGG numerical results

5.1. *Balanced and unbalanced initial data*

Here the interactions among only the IG modes (less the pure inertial modes) are considered via the GGG model. Before presenting numerical results, it may be of
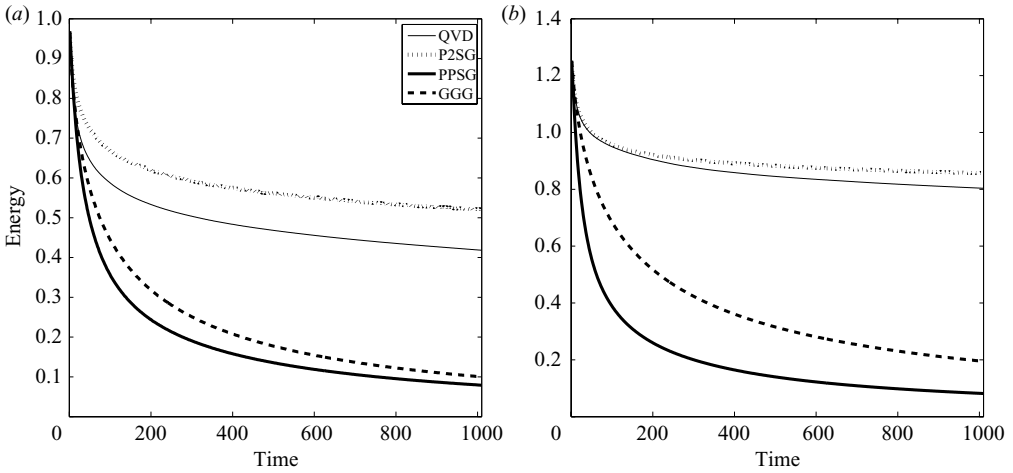
FIGURE 13. $Ro = .4$ and $Fr = .25$. Representative behaviour of the energy for the different models. (*a*) A100 initial conditions. (*b*) Balanced initial conditions.
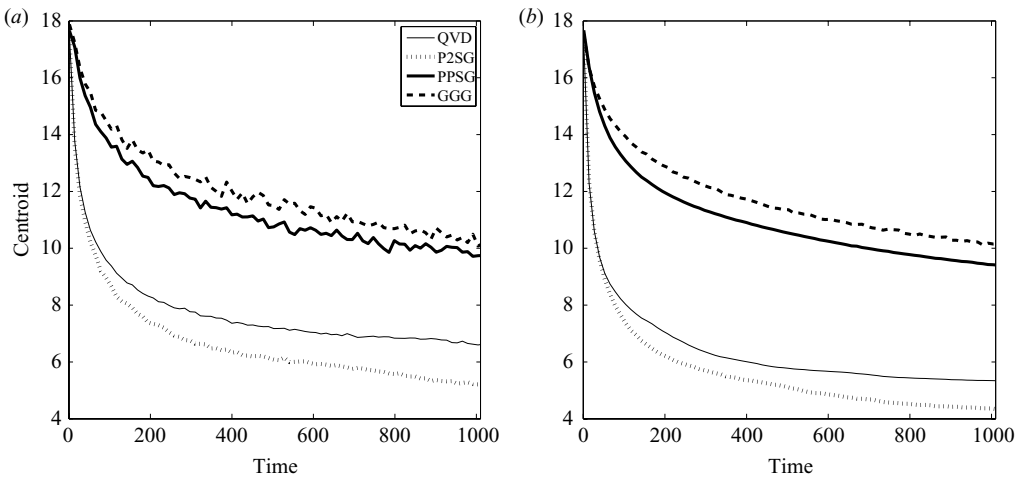

FIGURE 14. $Ro = .4$ and $Fr = .25$. Representative behaviour of the centroid for the different models. (*a*) A100 initial conditions. (*b*) Balanced initial conditions.

interest to note that the GGG model can be integrated with fewer Fourier transforms than RSW per time step. For A100 initial conditions, the skewness (figure 15) falls slightly negative before moving back towards zero. For balanced initial data, the skewness (figure 16) jumps to positive values before falling slightly and levelling off. The interactions among the IG modes do not replicate the general cyclone/anticyclone asymmetry of RSW. In addition, for both initial conditions, the interactions among the IG modes dissipate energy at a faster rate (figure 13) and do not lead to the growth in structures (figure 14) as for the models with the interactions among the vortical modes present. Based on the results of QG and GGG, we expect that a model that includes the interactions among the vortical modes along with the interactions among the IG modes would not give the asymmetry found in RSW or PPG, in part because there is no exchange between vortical and IG modes.
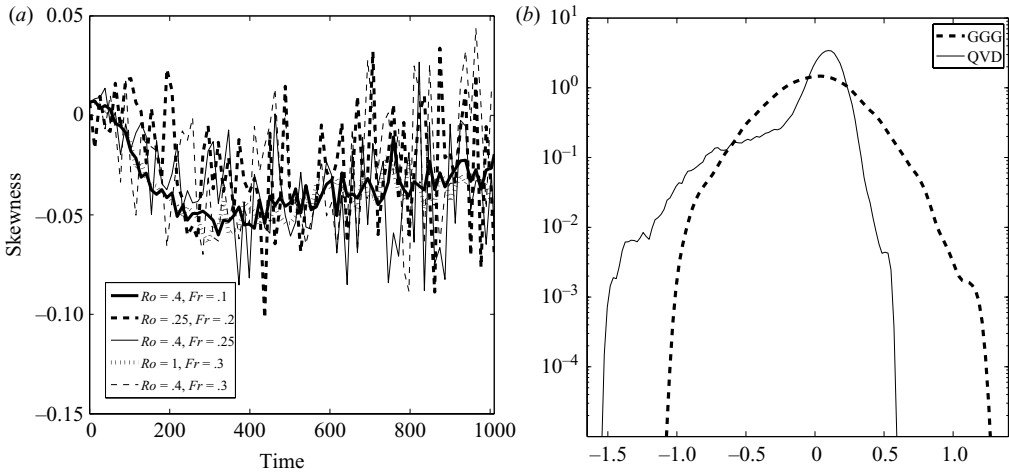
FIGURE 15. Unbalanced initial conditions. (*a*) Skewness versus time for GGG. (*b*) p.d.f. at about 500 turnover times comparison between QVD and GGG for $Ro = .4$ and $Fr = .25$.
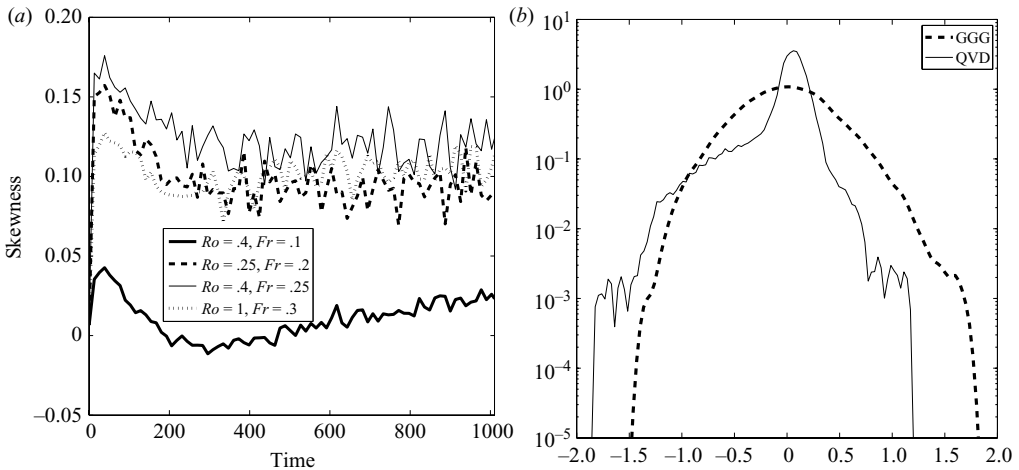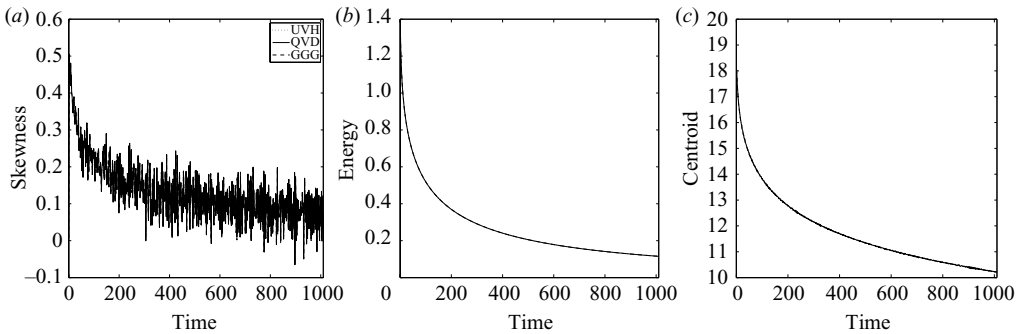

FIGURE 16. Balanced initial conditions. (*a*) Skewness versus time for GGG. (*b*) p.d.f. at about 500 turnover times comparison between QVD and GGG for $Ro = .4$ and $Fr = .25$.

5.2. *No initial linear PV data*

In Mohebalhojeh & Dritschel (2001) it is shown that the linear subspace of IG modes is an invariant manifold (this fact is also contained in Warn 1986). This is done using the Lagrangian invariant q and the fact that the linear IG modes contain none of the quantity $q - f/H$. The result can also be seen immediately by Fourier mode interactions. The interaction coefficients C_{kpq}^{0+-}, C_{kpq}^{0++} and C_{kpq}^{0--} (k, p and q all non-zero here) are all zero (appendix A, see also, Warn 1986). The linear subspace of IG modes not including the pure inertial modes is not an invariant manifold because a pure inertial mode can be generated by this subspace since $C_{0k-k}^{++-} \neq 0$ and $C_{0k-k}^{--+} \neq 0$ (see appendix A). However, the additional fact that C_{k0k}^{0++}, C_{k0k}^{0+-} and C_{k0k}^{0--} are also all zero shows that the linear subspace of IG modes is an invariant manifold. Therefore, by relation (3.6), if we start with no linear PV, then none can be generated. Hence,

Run	Fr	Ro	B	Model	Min. skewness	Max. kurtosis	Min. centroid
n	.1	.4	16	RSW	-1.6122	16.0612	3.2264
				PPG	-1.5797	12.4914	3.5612
				P2G	-1.2275	13.5751	3.7106
e	.2	.25	1.5625	RSW	-0.5560	4.2548	7.3701
				PPG	-0.3886	3.8522	7.8341
				P2G	-0.3170	3.6695	7.7687
q	.25	.4	2.560	RSW	-1.3550	6.2448	6.1077
				PPG	-0.8149	4.8067	6.9869
				P2G	-0.8613	4.8372	6.8285
s	.3	.4	1.7778	RSW	-0.9253	4.9214	6.8070
				PPG	-0.5546	3.8504	8.0028
				P2G	-0.4606	3.9074	7.6998
g	.3	1	11.1111	RSW	-2.9768	15.1632	4.3398
				PPG	-2.4794	11.8409	4.7660
				P2G	-2.4018	12.0015	4.4778

TABLE 3. Unbalanced 50 % divergence-free initial data.

FIGURE 17. $Ro = .13$ and $Fr = .3$. No PV initial conditions. (*a*) Skewness versus time. (*b*) Energy versus time. (*c*) Centroid versus time.

with initial data void of linear PV, GGG should give the same results as RSW. To obtain initial data with no linear PV, a random Ψ was generated as done for the balanced initial conditions, but then $Q = 0$ was inverted to obtain h. In order to satisfy the limit set on h by H (the perturbation depth cannot be below the mean depth) a large enough f is needed so that Ro is limited in magnitude. The numerical data show that the results obtained for GGG and RSW are indeed the same for this initial data (figure 17). Note with this initial data that the skewness becomes positive then fades back to zero with time.

5.3. *Further role of GGG interactions*

With the balanced and A100 initial conditions there are relatively minor differences in the qualitative behaviour between PPG, P2G and RSW. In order to learn about the role of the interactions between one vortical mode and two IG modes and among three IG modes, initial conditions that project stronger onto the gravity wave modes are used. This is done by decreasing the amount of energy that is initially divergence free from 100 % to 50 %, initial conditions A50. Results for initial conditions A50 are recorded in table 3. All runs are less skewed with initial conditions A50 than the corresponding runs for A100. In addition, the change in skewness between the
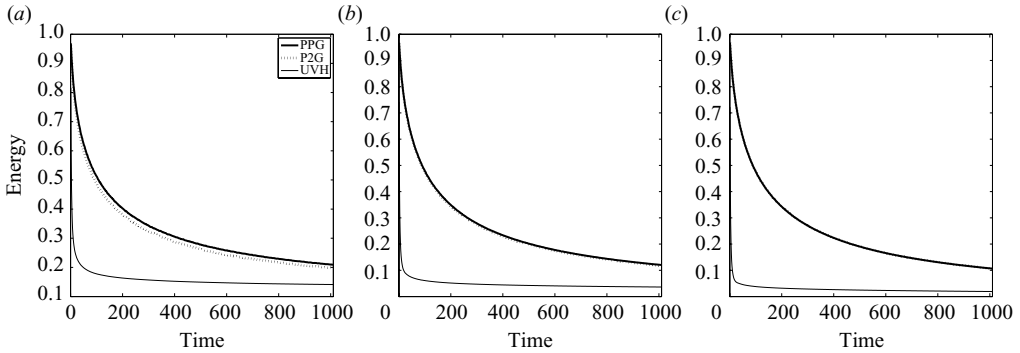
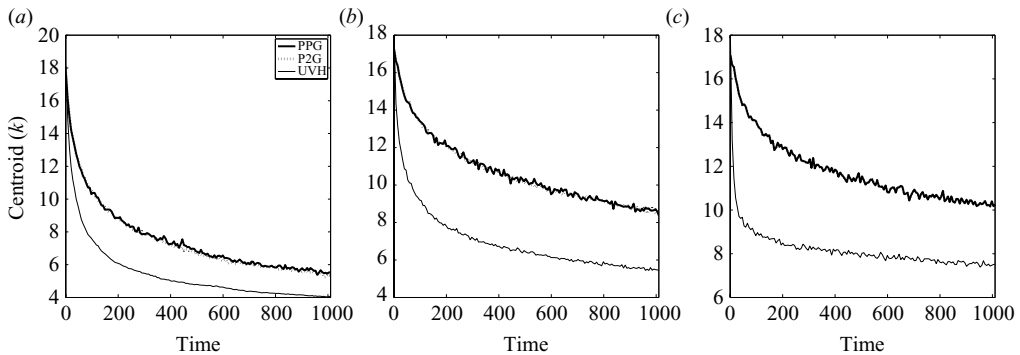FIGURE 18. $Ro = 1$ and $Fr = .3$. Energy versus time. (*a*) A25. (*b*) A5. (*c*) A0.

FIGURE 19. $Ro = 1$ and $Fr = .3$. Centroid versus time. (*a*) A25. (*b*) A5. (*c*) A0.

two initial conditions varies with the parameters of the flow and it appears that the change is greater for runs with a smaller Burger number. For example, looking at RSW, for run *e* the new minimum value of skewness is 44 % of the old, whereas for run *g* it is 89 %. Furthermore, the difference between the statistics of RSW and the other two models is now distinct with the A50 initial conditions, thereby singling out the additional role of the interactions among three IG modes. Observe that with initial conditions A50, RSW is the most skewed model for every run, including for run *n*; for balanced and A100 initial conditions, RSW was the least skewed for the parameter values of run *n*. In addition, RSW attains the greatest kurtosis and least centroid for each run compared to PPG and P2G. The differences between PPG and P2G as with the previous initial conditions are not very distinct. However, for all runs except run *q*, PPG attains a greater negative value of the skewness than P2G.

The results for initial conditions A25, A5 and A0 are found in figures 18–21. The results for A25 initial data accentuate those discussed for A50. Again RSW easily attains the most negative skewness, the largest kurtosis and the smallest centroid. The differences between PPG and P2G are even less distinct. Note that initial conditions A0 have zero projection onto the vortical modes; therefore, they are on the invariant manifold spanned by the linear subspace of IG modes. Hence, it is interesting to note the changes between initial conditions A5 and A0, in particular in the plots of the skewness (figure 21) and the kurtosis (figure 20). The resulting kurtosis of RSW for A5 initial conditions tends to increase throughout the run; for A0 initial conditions the kurtosis jumps above the value for a Gaussian before moving closer to this value with
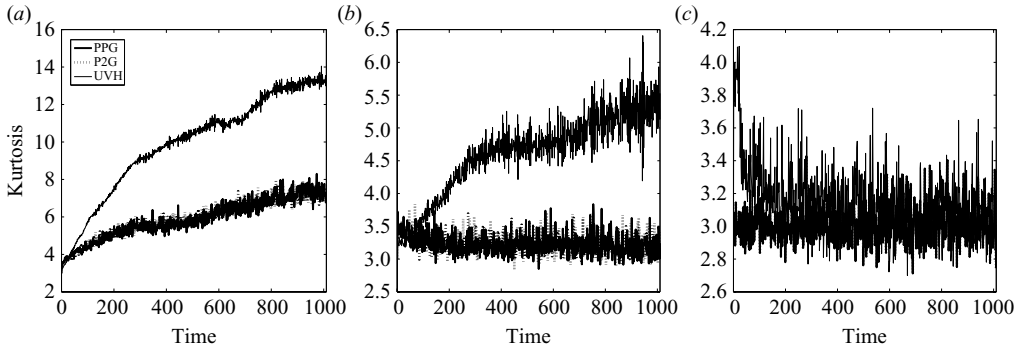
FIGURE 20. $Ro = 1$ and $Fr = .3$. Kurtosis versus time. (*a*) A25. (*b*) A5. (*c*) A0.
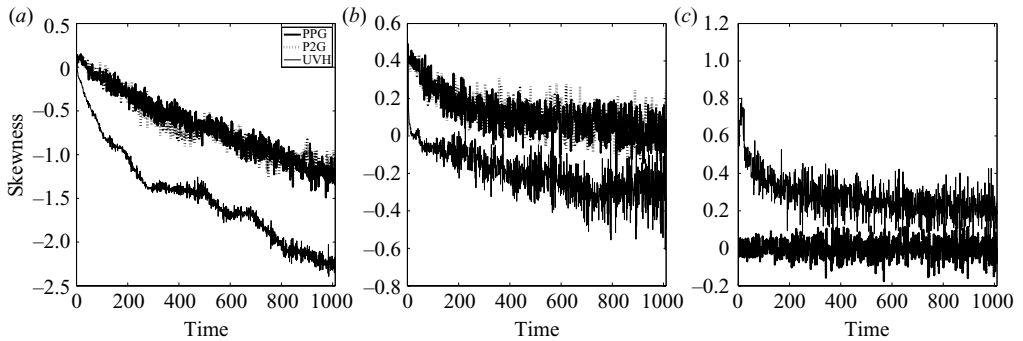

FIGURE 21. $Ro = 1$ and $Fr = .3$. Skewness versus time. (*a*) A25. (*b*) A5. (*c*) A0.

time. For the A5 initial conditions, the resulting skewness of RSW is always below that of the other models and attains negative values; whereas for A0 initial conditions the resulting skewness of RSW is positive and always above that of the other models. For A0 initial conditions PPG and P2G give the same result, one of pure decay without nonlinear interactions, a consequence of starting on the invariant manifold.

6. Conclusion and discussion

New intermediate models were developed for RSW by considering subsets of the interactions among the linear eigenmodes. These models are useful to determine the dynamical effects of certain mode interactions in various parameter regimes. In particular, several models were used here to explore cyclone/anticyclone asymmetry in RSW decay, including QG (vortical mode interactions only), PPG (vortical mode interactions and interactions among two vortical modes and one IG mode) and P2G (vortical mode interactions and interactions of vortical modes with one or two IG modes). Through the use of numerical experiments, it was found that PPG interactions are grossly responsible for the development of anticyclone dominance starting from unbiased balanced or unbiased unbalanced divergence-free initial conditions in a parameter range away from $Ro \rightarrow 0$. As divergence was added to the unbalanced initial conditions, the interactions among three IG modes played a larger role and separated the results for RSW from the models PPG and P2G. When the initial conditions contained significant divergence, the RSW had a greater dominance of anticyclones than PPG or P2G. No major differences were found between the PPG

and P2G models. Since the quadratic interaction of two IG modes to force a vortical mode is always zero, P2G adds to PPG only the interactions which change the amplitude of an IG mode by the interaction of an IG mode and a vortical mode. By definition these interactions are catalytic and include resonant catalytic interactions (opposite signed IG modes of the same wave shell).

The centroid and kurtosis were reported as a measure of the size and intermittency of the structures, respectively. For RSW, the smaller the size of the initial structures relative to the Rossby radius of deformation, the more the structures were found to grow as reported in Polvani *et al.* (1994) (i.e. a larger initial *Bu* is associated with more of an increase in structure size). This was also the general trend for the models PPG and P2G. For PPG, P2G and RSW, the initial conditions influenced the growth of structures, with the larger structures developing from balanced initial conditions. In the models that do not include the QG interactions among three vortical modes, not surprisingly, the growth of larger structures was restricted. The QG model, also not surprisingly, had the largest growth in the structures. For all initial conditions considered herein, as for the skewness, PPG and P2G exhibited relatively little difference for the size and intermittency of the structures. We expect differences for the corresponding RBE models with regard to structure size since the interactions are less restricted (see below).

We have also performed forced experiments starting from rest to compare the QG, PPG, P2G model dynamics to the full RSW forced dynamics. We used a random white-in-time force with Gaussian spatial correlation localized about a given wavenumber, and explored various scenarios: forcing of only the vortical modes, only the IG modes, all modes and only a divergence-free velocity field. Interesting results were obtained for the QG, PPG, P2G and RSW models when only the vortical modes were forced at small scales, but relatively far from the dissipation range. First, all four models had approximately a linear increase of energy with time, with total energy approximately equal to the product of the energy input rate multiplied by the elapsed time. Second, all models showed virtually the same growth of the structures with time. However, the skewness of the QG model remained roughly zero. In contrast, the skewness of the PPG, P2G and RSW became negative, again indicating a bias for anticyclones. All three systems PPG, P2G and RSW exhibited approximately the same quantitative development of the negative skewness. Differences arise between RSW and the PPG and P2G models when all modes are forced and when only the IG modes are forced. These results will be presented in detail elsewhere.

In addition, this type of work is applicable to other systems. For example, the authors have derived the analogous models for RBE as presented here for RSW. These RBE models could be even more illuminating for several reasons. The hydrostatic and 'thin layer' assumptions in RSW have the effect of limiting resonant and/or near resonant interactions. In particular, RSW is known to lack resonant interactions among three IG modes (Warn 1986; Embid & Majda 1996). Since the thin layer and hydrostatic assumptions are absent from RBE, our intermediate models could potentially help to distinguish between different classes of exact and near resonant interactions. For example, it is known that the vortical mode interactions dominate the dynamics for strong rotation and stratification in the range $1/2 \leqslant N/f \leqslant 2$ (also the range for which resonant interactions among IG modes do not exist in RBE Bartello 1995; Embid & Majda 1998; Babin, Mahalov & Nicolaenko 2000; Smith & Waleffe 2002; Sukhatme & Smith 2008). For $N/f > 2$, $Ro = O(1)$ and forcing at small scales, previous numerical work indicated the important role of the IG modes in the formation of Vertically Sheared Horizontal Flows (VSHF), but did not distinguish

between the role of three IG wave interactions and interactions involving two IG modes and one vortical mode (Smith & Waleffe 2002). Analytical and numerical calculations have suggested that the catalytic near resonances play a key role in establishing qualitatively different dynamics for $N/f > 2$ and $N/f < 1/2$ (Bartello 1995; Babin *et al.* 2000; Smith & Waleffe 2002; Sukhatme & Smith 2008). With our hierarchy of models, we have the ability to explore the origin of such differences through study of mode coupling, for all possible classes of mode interactions, in isolation and in concert. Analysis of the model coupling coefficients and numerical calculations should significantly increase our understanding of important phenomena such as asymmetry and loss of balance.

Appendix A. Interaction coefficients

The interaction coefficients are determined in the calculation of the right-hand side of (2.17) restricted to the interaction of the certain modes of the coefficient. The interaction coefficient depends on the way in which it is defined. In this paper the interaction coefficient $C_{kpq}^{\alpha\beta\gamma}$ is defined by

$$\frac{\partial a_k^\alpha}{\partial t} + i\omega_k^\alpha a_k^\alpha = \frac{1}{\sqrt{H}} \sum_{\beta,\gamma} \sum_{k=p+q} a_p^\beta a_q^\gamma C_{kpq}^{\alpha\beta\gamma}. \tag{A 1}$$

Another possible definition analogous to that used by Warn (1986) is

$$\frac{\partial a_k^\alpha}{\partial t} + i\omega_k^\alpha a_k^\alpha = \frac{i}{\sqrt{H}} \sum_{\beta,\gamma} \sum_{k+p+q=0} \overline{a_p^\beta a_q^\gamma} \mu_{kpq}^{\alpha\beta\gamma}. \tag{A 2}$$

The coefficients are related by

$$\mu_{kpq}^{\alpha\beta\gamma} = -i C_{k-p-q}^{\alpha-\beta-\gamma}. \tag{A 3}$$

Using the reality conditions, the radial property of the dispersion relation and that $\omega_k^{-\alpha} = -\omega_k^\alpha$, it is easy to show that

$$C_{kpq}^{-\alpha-\beta-\gamma} = \overline{C_{-k-p-q}^{\alpha\beta\gamma}}. \tag{A 4}$$

A formula for the explicit calculation of the interaction coefficients is useful. Here we borrow some notation ideas from Warn (1986) and elect a symmetric definition. The notation $(\boldsymbol{u}, \boldsymbol{v})$ is used to represent $\sum u_i v_i$. Then, with the understanding that when a two-dimensional wavevector is used in a three-dimensional operation it is appended with a zero for its third component, define

$$I_{kpq}^{\alpha\beta\gamma} \equiv -(i\boldsymbol{p}, \boldsymbol{\phi}_q^\gamma)(\boldsymbol{\phi}_p^\beta, \overline{\boldsymbol{\phi}_k^\alpha}) - (i\boldsymbol{p}, \boldsymbol{\phi}_p^\beta)(\hat{z}, \boldsymbol{\phi}_q^\gamma)(\hat{z}, \overline{\boldsymbol{\phi}_k^\alpha}), \tag{A 5}$$

so that

$$C_{kpq}^{\alpha\beta\gamma} = \frac{I_{kpq}^{\alpha\beta\gamma} + I_{kqp}^{\alpha\gamma\beta}}{2}. \tag{A 6}$$

Next the interaction coefficient corresponding to $0|0+$ is calculated directly as an illustration. Consider one triad $\boldsymbol{k} = \boldsymbol{p} + \boldsymbol{q}$, which does not contain the zero vector. Let $\boldsymbol{k}$ and $\boldsymbol{p}$ be vortical modes and $\boldsymbol{q}$ be an IG mode. We calculate $-(\widehat{NL}_{\boldsymbol{k}} \cdot \boldsymbol{\phi}_{\boldsymbol{k}}^0)\sqrt{H}$ for this triad,

$$
-\Big[(\mathrm{i}\boldsymbol{p} \cdot (\psi_1(\boldsymbol{q})), \psi_2(\boldsymbol{q}))\boldsymbol{\phi}^0(\boldsymbol{p}) + (\mathrm{i}\boldsymbol{q}) \cdot (\psi_1(\boldsymbol{p}), \psi_2(\boldsymbol{p}))\boldsymbol{\phi}^+(\boldsymbol{q})
$$

$$
+ \begin{pmatrix} 0 \\ 0 \\ \psi_3(\boldsymbol{p})(\mathrm{i}\boldsymbol{q} \cdot (\psi_1(\boldsymbol{q}), \psi_2(\boldsymbol{q}))) \end{pmatrix} + \begin{pmatrix} 0 \\ 0 \\ \psi_3(\boldsymbol{q})(\mathrm{i}\boldsymbol{p} \cdot (\psi_1(\boldsymbol{p}), \psi_2(\boldsymbol{p}))) \end{pmatrix} \Big] \cdot \boldsymbol{\phi}_{\boldsymbol{k}}^0 \quad \text{(A\,7)}
$$

$$
= -\frac{a^0(\boldsymbol{p})a^+(\boldsymbol{q})}{\sqrt{2}\omega_p\omega_q q\omega_k} \Big\{ (\mathrm{i}\omega_q \boldsymbol{p} \cdot \boldsymbol{q} + f(\boldsymbol{q} \times \boldsymbol{p} \cdot \hat{z})) \begin{pmatrix} -\mathrm{i}p_y c \\ \mathrm{i}p_x c \\ f \end{pmatrix} + c(\boldsymbol{q} \times \boldsymbol{p} \cdot \hat{z})
$$

$$
\begin{pmatrix} \omega_q q_x + \mathrm{i}fq_y \\ \omega_q q_y - \mathrm{i}fq_x \\ cq^2 \end{pmatrix} + \begin{pmatrix} 0 \\ 0 \\ \mathrm{i}f\omega_q q^2 \end{pmatrix} \Big\} \cdot \begin{pmatrix} \mathrm{i}k_y c \\ -\mathrm{i}k_x c \\ f \end{pmatrix}. \quad \text{(A\,8)}
$$

Simplifying, one obtains

$$
\frac{a_p^0 a_q^+}{\sqrt{2}\omega_p\omega_q q\omega_k} \big(f(\boldsymbol{p} \times \boldsymbol{q} \cdot \hat{z})\omega_p^2 - \mathrm{i}\omega_q\omega_p^2(\boldsymbol{p} \cdot \boldsymbol{q} + q^2) \big) \qquad \text{for } \boldsymbol{k} = \boldsymbol{p} + \boldsymbol{q}. \quad \text{(A\,9)}
$$

Including all triads results in

$$
\frac{\partial a_k^0}{\partial t} = \frac{1}{\sqrt{H}} \sum_{\triangle} \frac{\overline{a_p^0 a_q^-}}{\sqrt{2}\omega_p\omega_q q\omega_k} \big(f(\boldsymbol{p} \times \boldsymbol{q} \cdot \hat{z})\omega_p^2 - \mathrm{i}\omega_q\omega_p^2(\boldsymbol{p} \cdot \boldsymbol{q} + q^2) \big). \quad \text{(A\,10)}
$$

Therefore

$$
C_{kpq}^{00+} = \frac{1}{2\sqrt{2}\omega_p\omega_q q\omega_k} \big(f(\boldsymbol{p} \times \boldsymbol{q} \cdot \hat{z})\omega_p^2 - \mathrm{i}\omega_q\omega_p^2(\boldsymbol{p} \cdot \boldsymbol{q} + q^2) \big); \quad \text{(A\,11)}
$$

the factor of $1/2$ appears due to the sum over β and γ in A 1 and there is an equal contribution from C_{kpq}^{0+0}, however, (A 10) as written does take care of the contributions from C_{kpq}^{00+} and C_{kpq}^{0+0}.

Now let $\boldsymbol{k} \to -\boldsymbol{k}$, $\boldsymbol{p} \to -\boldsymbol{p}$, $\boldsymbol{q} \to -\boldsymbol{q}$ and use reality to obtain

$$
\frac{\partial \overline{a_k^0}}{\partial t} = \frac{1}{\sqrt{H}} \sum_{\triangle} \frac{a_p^0 a_q^+}{\sqrt{2}\omega_p\omega_q q\omega_k} \big(f(\boldsymbol{p} \times \boldsymbol{q} \cdot \hat{z})\omega_p^2 - \mathrm{i}\omega_q\omega_p^2(\boldsymbol{p} \cdot \boldsymbol{q} + q^2) \big). \quad \text{(A\,12)}
$$

Taking the complex conjugate obtains

$$
\frac{\partial a_k^0}{\partial t} = \frac{1}{\sqrt{H}} \sum_{\triangle} \frac{\overline{a_p^0 a_q^+}}{\sqrt{2}\omega_p\omega_q q\omega_k} \big(f(\boldsymbol{p} \times \boldsymbol{q} \cdot \hat{z})\omega_p^2 + \mathrm{i}\omega_q\omega_p^2(\boldsymbol{p} \cdot \boldsymbol{q} + q^2) \big). \quad \text{(A\,13)}
$$

Therefore

$$
C_{kpq}^{00-} = \frac{1}{2\sqrt{2}\omega_p\omega_q q\omega_k} \big(f(\boldsymbol{p} \times \boldsymbol{q} \cdot \hat{z})\omega_p^2 + \mathrm{i}\omega_q\omega_p^2(\boldsymbol{p} \cdot \boldsymbol{q} + q^2) \big), \quad \text{(A\,14)}
$$

which agrees with the result obtained from (A 4) applied to (A 11). Now we complete the list

$$C_{kpq}^{000} = \frac{1}{\omega_p \omega_q \omega_k} c(\boldsymbol{p} \times \boldsymbol{q} \cdot \hat{z}) \left(\frac{\omega_q^2 - \omega_p^2}{2} \right), \tag{A 15}$$

$$C_{kpq}^{0++} = 0, \tag{A 16}$$

$$C_{kpq}^{0+-} = 0, \tag{A 17}$$

$$C_{kpq}^{+00} = \frac{1}{2\sqrt{2}\omega_p \omega_q \omega_k k} \left(f(\boldsymbol{p} \times \boldsymbol{q} \cdot \hat{z})(\omega_p^2 - \omega_q^2) - 2i\omega_k c^2 (\boldsymbol{p} \times \boldsymbol{q} \cdot \hat{z})^2 \right), \tag{A 18}$$

$$C_{kpq}^{+0+} = \frac{1}{2\omega_p \omega_q q \omega_k k} \frac{1}{2} \left\{ \frac{1}{c} (\boldsymbol{p} \times \boldsymbol{q} \cdot \hat{z})\omega_q^2 \omega_k^2 + \frac{f^2}{c} (\boldsymbol{q} \times \boldsymbol{p} \cdot \hat{z})\omega_p^2 - if c\omega_q (q^4 + 3(\boldsymbol{p} \cdot \boldsymbol{q})q^2 \right.$$
$$\left. + 2(\boldsymbol{p} \cdot \boldsymbol{q})^2) + 2if c\omega_k (\boldsymbol{p} \times \boldsymbol{q} \cdot \hat{z})^2 - \omega_q \omega_k c(\boldsymbol{q} \times \boldsymbol{p} \cdot \hat{z})(q^2 + 2(\boldsymbol{p} \cdot \boldsymbol{q})) \right\}, \tag{A 19}$$

$$C_{kpq}^{+0-} = \frac{1}{2\omega_p \omega_q q \omega_k k} \frac{1}{2} \left\{ \frac{1}{c} (\boldsymbol{p} \times \boldsymbol{q} \cdot \hat{z})\omega_q^2 \omega_k^2 + \frac{f^2}{c} (\boldsymbol{q} \times \boldsymbol{p} \cdot \hat{z})\omega_p^2 + if c\omega_q (q^4 + 3(\boldsymbol{p} \cdot \boldsymbol{q})q^2 \right.$$
$$\left. + 2(\boldsymbol{p} \cdot \boldsymbol{q})^2) + 2if c\omega_k (\boldsymbol{p} \times \boldsymbol{q} \cdot \hat{z})^2 + \omega_q \omega_k c(\boldsymbol{q} \times \boldsymbol{p} \cdot \hat{z})(q^2 + 2(\boldsymbol{p} \cdot \boldsymbol{q})) \right\}, \tag{A 20}$$

$$C_{kpq}^{+++} = \frac{1}{2\sqrt{2}\omega_p p \omega_q q \omega_k k} \frac{1}{2} \left\{ - f\omega_k \omega_q (\boldsymbol{p} \times \boldsymbol{q} \cdot \hat{z})(q^2 + 2(\boldsymbol{p} \cdot \boldsymbol{q})) + f\omega_k \omega_p (\boldsymbol{p} \times \boldsymbol{q} \cdot \hat{z}) \right.$$
$$\times (p^2 + 2(\boldsymbol{p} \cdot \boldsymbol{q})) - f\omega_k^2 (\boldsymbol{p} \times \boldsymbol{q} \cdot \hat{z})(q^2 - p^2) - i\omega_k^2 \omega_p q^2 (\boldsymbol{p} \cdot \boldsymbol{q} + p^2)$$
$$\left. - i\omega_k^2 \omega_q p^2 (\boldsymbol{p} \cdot \boldsymbol{q} + q^2) - i\omega_p \omega_q \omega_k k^2 (\boldsymbol{p} \cdot \boldsymbol{q}) - 2if^2 \omega_k (\boldsymbol{p} \times \boldsymbol{q} \cdot \hat{z})^2 \right\}, \tag{A 21}$$

$$C_{kpq}^{+-+} = \frac{1}{2\sqrt{2}\omega_p p \omega_q q \omega_k k} \frac{1}{2} \left\{ - f\omega_k \omega_q (\boldsymbol{p} \times \boldsymbol{q} \cdot \hat{z})(q^2 + 2(\boldsymbol{p} \cdot \boldsymbol{q})) - f\omega_k \omega_p (\boldsymbol{p} \times \boldsymbol{q} \cdot \hat{z}) \right.$$
$$\times (p^2 + 2(\boldsymbol{p} \cdot \boldsymbol{q})) - f\omega_k^2 (\boldsymbol{p} \times \boldsymbol{q} \cdot \hat{z})(q^2 - p^2) + i\omega_k^2 \omega_p q^2 (\boldsymbol{p} \cdot \boldsymbol{q} + p^2)$$
$$\left. - i\omega_k^2 \omega_q p^2 (\boldsymbol{p} \cdot \boldsymbol{q} + q^2) + i\omega_p \omega_q \omega_k k^2 (\boldsymbol{p} \cdot \boldsymbol{q}) - 2if^2 \omega_k (\boldsymbol{p} \times \boldsymbol{q} \cdot \hat{z})^2 \right\}, \tag{A 22}$$

$$C_{kpq}^{+--} = \frac{1}{2\sqrt{2}\omega_p p \omega_q q \omega_k k} \frac{1}{2} \left\{ f\omega_k \omega_q (\boldsymbol{p} \times \boldsymbol{q} \cdot \hat{z})(q^2 + 2(\boldsymbol{p} \cdot \boldsymbol{q})) - f\omega_k \omega_p (\boldsymbol{p} \times \boldsymbol{q} \cdot \hat{z}) \right.$$
$$\times (p^2 + 2(\boldsymbol{p} \cdot \boldsymbol{q})) - f\omega_k^2 (\boldsymbol{p} \times \boldsymbol{q} \cdot \hat{z})(q^2 - p^2) + i\omega_k^2 \omega_p q^2 (\boldsymbol{p} \cdot \boldsymbol{q} + p^2)$$
$$\left. + i\omega_k^2 \omega_q p^2 (\boldsymbol{p} \cdot \boldsymbol{q} + q^2) - i\omega_p \omega_q \omega_k k^2 (\boldsymbol{p} \cdot \boldsymbol{q}) - 2if^2 \omega_k (\boldsymbol{p} \times \boldsymbol{q} \cdot \hat{z})^2 \right\}. \tag{A 23}$$

The non-zero mean flow interactions are

$$C_{kk0}^{00+} = \frac{1}{\sqrt{2}} (k_x - ik_y), \tag{A 24}$$

$$C_{0-kk}^{+0+} = \frac{1}{2\omega_k} kc(k_x + ik_y), \tag{A 25}$$

$$C_{0-kk}^{+0-} = \frac{1}{2\omega_k} kc(-k_x - ik_y), \tag{A 26}$$

$$C_{kk0}^{+++} = \frac{1}{\sqrt{2}}(k_x - \mathrm{i}k_y), \tag{A 27}$$

$$C_{kk0}^{++-} = \frac{1}{\sqrt{2}}(-k_x - \mathrm{i}k_y), \tag{A 28}$$

$$C_{0k-k}^{++-} = \frac{1}{\sqrt{2}\omega_k} f(-k_x - \mathrm{i}k_y). \tag{A 29}$$

Here reality, $a^+(\mathbf{0}) = \overline{a^-(\mathbf{0})}$, can be used as well to complete the list. Many interactions including mean flows are zero: C_{k0k}^{0++}, C_{k0k}^{0+-}, C_{k0k}^{++0}, C_{k0k}^{+-0}, C_{0k-k}^{+00}, C_{0k-k}^{+++}, C_{0k-k}^{+--}, C_{kk0}^{++}, and C_{kk0}^{+--}.

Appendix B. Detailed balance

LEMMA 1. *Consider the system* $\partial \mathbf{u}/\partial t + L(\mathbf{u}) + B(\mathbf{u}, \mathbf{u}) = 0$, *which has* $\int \mathbf{u} \cdot \mathbf{u}\mathrm{d}\mathbf{x}$ *as a quadratic invariant and the linear operator, L, has orthogonal eigenvectors with purely imaginary eigenvalues corresponding to modes* α, β *and* γ. *Then, for a triad* $\mathbf{k} + \mathbf{p} + \mathbf{q} = 0$, *the interaction coefficients sum to zero.*

$$C_{kpq}^{\alpha\beta\gamma} + C_{pqk}^{\beta\gamma\alpha} + C_{qkp}^{\gamma\alpha\beta} = 0$$

Proof. This is a generalization of the idea found in Kraichnan (1973, §3) Make the eigenfunctions orthonormal and write

$$\mathbf{u} = \sum_k \{a_k^\alpha \boldsymbol{\phi}_k^\alpha + a_k^\beta \boldsymbol{\phi}_k^\beta + a_k^\gamma \boldsymbol{\phi}_k^\gamma\}\mathrm{e}^{\mathrm{i}\mathbf{k}\cdot\mathbf{x}}.$$

Therefore,

$$\int \mathbf{u} \cdot \mathbf{u}\mathrm{d}\mathbf{x} = \int \left(\sum_k \{a_k^\alpha \boldsymbol{\phi}_k^\alpha + a_k^\beta \boldsymbol{\phi}_k^\beta + a_k^\gamma \boldsymbol{\phi}_k^\gamma\}\mathrm{e}^{\mathrm{i}\mathbf{k}\cdot\mathbf{x}} \sum_l \{a_l^\alpha \boldsymbol{\phi}_l^\alpha + a_l^\beta \boldsymbol{\phi}_l^\beta + a_l^\gamma \boldsymbol{\phi}_l^\gamma\}\mathrm{e}^{\mathrm{i}\mathbf{l}\cdot\mathbf{x}} \right) \mathrm{d}\mathbf{x}.$$

Using the invariance of this quantity leads to the result

$$\frac{\mathrm{d}}{\mathrm{d}t}\left(\sum_k |a_k^\alpha|^2 + |a_k^\beta|^2 + |a_k^\gamma|^2 \right) = 0. \tag{B 1}$$

Initially let only the amplitude of exactly one mode for each leg of a single triad, $\mathbf{k} + \mathbf{p} + \mathbf{q} = 0$, be non-zero. For the $\mathbf{k}$ leg the δ mode and the ϵ mode and ζ mode for the $\mathbf{p}$ and $\mathbf{q}$ legs, respectively, where δ, ϵ and ζ are one of α, β or γ. Therefore, at time zero (B 1) yields

$$\left(\frac{\partial a_k^\delta}{\partial t}\overline{a_k^\delta} + \frac{\partial a_p^\epsilon}{\partial t}\overline{a_p^\epsilon} + \frac{\partial a_q^\zeta}{\partial t}\overline{a_q^\zeta} + C.C. \right) = 0,$$

or

$$\left(-\mathrm{i}\sigma_k^\delta a_k^\delta \overline{a_k^\delta} - \mathrm{i}\sigma_p^\epsilon a_p^\epsilon \overline{a_p^\epsilon} - \mathrm{i}\sigma_q^\zeta a_q^\zeta \overline{a_q^\zeta} + \overline{a_k^\delta}\,\overline{a_p^\epsilon}\,\overline{a_q^\zeta} \{C_{kpq}^{\delta\epsilon\zeta} + C_{pqk}^{\epsilon\zeta\delta} + C_{qkp}^{\zeta\delta\epsilon}\} \right) + C.C. = 0,$$

where *C.C.* is short for complex conjugate.
Hence,

$$\overline{a_k^\delta}\,\overline{a_p^\epsilon}\,\overline{a_q^\zeta} \{C_{kpq}^{\delta\epsilon\zeta} + C_{pqk}^{\epsilon\zeta\delta} + C_{qkp}^{\zeta\delta\epsilon}\} + C.C. = 0.$$

$\square$

Appendix C. Fourier space representation of P2G and GGG

C.1. *P2G*

As similarly done for PPG, add and subtract (3.25) and (3.26)

$$\frac{\partial(a_k^+ + a_k^-)}{\partial t} + i\omega_k(a_k^+ - a_k^-) = \frac{1}{\sqrt{H}} \sum_{k+p+q=0} \frac{\overline{a_p^0}}{\omega_p\omega_q\omega_k k} \left\{ \frac{\overline{a_q^0}}{\sqrt{2}} f(\boldsymbol{p} \times \boldsymbol{q} \cdot \hat{z})(\omega_p^2 - \omega_q^2) \right.$$

$$+ \left(\frac{\overline{a_q^+ + a_q^-}}{q}\right)\left[\frac{1}{c}(\boldsymbol{p} \times \boldsymbol{q} \cdot \hat{z})\omega_q^2\omega_k^2 - \frac{f^2}{c}(\boldsymbol{p} \times \boldsymbol{q} \cdot \hat{z})\omega_p^2\right]$$

$$+ \left.\left(\frac{\overline{a_q^+ - a_q^-}}{q}\right)[\mathrm{i}fc\omega_q(q^4 + 3q^2(\boldsymbol{p} \cdot \boldsymbol{q}) + 2(\boldsymbol{p} \cdot \boldsymbol{q})^2)]\right\}, \qquad (C\,1)$$

$$\frac{\partial(a_k^+ - a_k^-)}{\partial t} + i\omega_k(a_k^+ + a_k^-) = \frac{1}{\sqrt{H}} \sum_{k+p+q=0} \frac{\overline{a_p^0}}{\omega_p\omega_q\omega_k k} \left\{ \frac{\overline{a_q^0}}{\sqrt{2}}[-2\mathrm{i}\omega_k c^2(\boldsymbol{p} \times \boldsymbol{q} \cdot \hat{z})^2] \right.$$

$$+ \frac{\overline{(a_q^+ + a_q^-)}}{q}[2\mathrm{i}fc\omega_k(\boldsymbol{p} \times \boldsymbol{q} \cdot \hat{z})^2] + \left.\frac{\overline{(a_q^+ - a_q^-)}}{q}[\omega_q\omega_k c(\boldsymbol{q} \times \boldsymbol{p} \cdot \hat{z})(q^2 + 2(\boldsymbol{p} \cdot \boldsymbol{q})]\right\}, \quad (C\,2)$$

$$\frac{\partial(a_0^+ + a_0^-)}{\partial t} + \mathrm{i}f(a_0^+ - a_0^-) = \frac{1}{\sqrt{H}} \sum_k a_{-k}^0\left(\frac{kck_x}{\omega_k}(a_k^+ - a_k^-)\right), \qquad (C\,3)$$

$$\frac{\partial(a_0^+ - a_0^-)}{\partial t} + \mathrm{i}f(a_0^+ + a_0^-) = \frac{1}{\sqrt{H}} \sum_k a_{-k}^0\left(\frac{kc\mathrm{i}k_y}{\omega_k}(a_k^+ - a_k^-)\right). \qquad (C\,4)$$

Note that the generation of mean flows separates into their own equations (C 3) and (C 4), where the sum on the right-hand side over the dummy variable $\boldsymbol{k}$ represents a domain average.

C.2. *GGG*

Add and subtract (3.32) and (3.33) to obtain

$$\frac{\partial(a_k^+ + a_k^-)}{\partial t} + i\omega_k(a_k^+ - a_k^-) = (a_k^+ + a_k^-)(-\mathrm{i}k_x u_0 - \mathrm{i}k_y v_0)$$

$$+ \frac{1}{\sqrt{H}} \sum_\triangle \frac{1}{\omega_k k}\left\{ \left(\frac{\overline{(a_p^+ + a_p^-)}}{\omega_p p}\right)\left(\frac{\overline{(a_q^+ + a_q^-)}}{2\sqrt{2}\omega_q q}\right)(-f\omega_k^2(\boldsymbol{p} \times \boldsymbol{q} \cdot \hat{z})(q^2 - p^2)) \right.$$

$$+ \left.\left(\frac{\overline{(a_p^+ + a_p^-)}}{\omega_p p}\right)\left(\frac{\overline{(a_q^+ - a_q^-)}}{2\sqrt{2}\omega_q q}\right)(2\mathrm{i}\omega_k^2\omega_q p^2(q^2 + \boldsymbol{p} \cdot \boldsymbol{q}))\right\}, \qquad (C\,5)$$

$$\frac{\partial(a_k^+ - a_k^-)}{\partial t} + i\omega_k(a_k^+ + a_k^-) = (a_k^+ - a_k^-)(-\mathrm{i}k_x u_0 - \mathrm{i}k_y v_0)$$

$$+ \frac{1}{\sqrt{H}} \sum_\triangle \frac{1}{\omega_k k}\left\{ \left(\frac{\overline{(a_p^+ + a_p^-)}}{\omega_p p}\right)\left(\frac{\overline{(a_q^+ + a_q^-)}}{2\sqrt{2}\omega_q q}\right) - 2\mathrm{i}f^2\omega_k(\boldsymbol{p} \times \boldsymbol{q} \cdot \hat{z})^2 \right.$$

$$+ \left(\frac{\overline{(a_p^+ + a_p^-)}}{\omega_p p}\right)\left(\frac{\overline{(a_q^+ - a_q^-)}}{2\sqrt{2}\omega_q q}\right)2f\omega_k\omega_q(\boldsymbol{p} \times \boldsymbol{q} \cdot \hat{z})(q^2 + 2\boldsymbol{p} \cdot \boldsymbol{q})$$

$$+ \left.\left(\frac{\overline{(a_p^+ - a_p^-)}}{\omega_p p}\right)\left(\frac{\overline{(a_q^+ - a_q^-)}}{2\sqrt{2}\omega_q q}\right)(-\mathrm{i}\omega_p\omega_q\omega_k \boldsymbol{p} \cdot \boldsymbol{q}k^2)\right\}, \qquad (C\,6)$$

$$\frac{\partial(a_0^+ - a_0^-)}{\partial t} + \mathrm{i}f(a_0^+ + a_0^-) = \frac{1}{\sqrt{H}} \sum_k -\frac{a_k^+ a_{-k}^-}{\omega_k} \sqrt{2} f \mathrm{i} k_y, \tag{C 7}$$

$$\frac{\partial(a_0^+ + a_0^-)}{\partial t} + \mathrm{i}f(a_0^+ - a_0^-) = \frac{1}{\sqrt{H}} \sum_k -\frac{a_k^+ a_{-k}^-}{\omega_k} \sqrt{2} f k_x, \tag{C 8}$$

Appendix D. Other reduced models

No mean flow interactions are considered here.

D.1. *P2SG (P2G less interactions with exactly one IG mode)*

Symbolically,

$$\frac{\partial a_k^0}{\partial t} = 00 \oplus + + \oplus + - \oplus - - \tag{D 1}$$

$$\frac{\partial a_k^+}{\partial t} + \mathrm{i}\omega_k a_k^+ = 0 + \oplus 0 - \tag{D 2}$$

$$\frac{\partial a_k^-}{\partial t} - \mathrm{i}\omega_k a_k^- = 0 + \oplus 0 - . \tag{D 3}$$

The resulting equations are

$$\frac{\partial Q}{\partial t} = J(A, Q), \tag{D 4}$$

$$\frac{\partial \nabla^2(f\Psi - gh)}{\partial t} - c^2 \nabla^4 \chi + f^2 \nabla^2 \chi = \nabla^2(J(A, V) - f(A\nabla^2 \chi + \nabla A \cdot \nabla \chi))$$
$$+ J(Q, c^2 \nabla^2 B) + f(\nabla^2 \chi \nabla^2 A + \nabla \chi \cdot \nabla \nabla^2 A) - J(\nabla^2 A, V), \tag{D 5}$$

$$\frac{\partial \nabla^2 \chi}{\partial t} - f\nabla^2 \psi + g\nabla^2 h = \nabla^2 J(A, \chi) - J(\nabla^2 A, \chi) + 2f(J(A_y, B_x) + J(B_y, A_x)). \tag{D 6}$$

D.2. *PPSG (PPG less the interactions among the vortical modes)*

Symbolically,

$$\frac{\partial a_k^0}{\partial t} = 0 + \oplus 0 - \tag{D 7}$$

$$\frac{\partial a_k^+}{\partial t} + \mathrm{i}\omega_k a_k^+ = 00 \tag{D 8}$$

$$\frac{\partial a_k^-}{\partial t} - \mathrm{i}\omega_k a_k^- = 00. \tag{D 9}$$

Leading to

$$\frac{\partial Q}{\partial t} = f J(Q, B) - \nabla Q \cdot \nabla \chi - Q\nabla^2 \chi \tag{D 10}$$

$$\frac{\partial \nabla^2(f\Psi - gh)}{\partial t} - c^2 \nabla^4 \chi + f^2 \nabla^2 \chi = f J(A, Q) \tag{D 11}$$

$$\frac{\partial \nabla^2 \chi}{\partial t} - f\nabla^2 \psi + g\nabla^2 h = 2J(A_x, A_y). \tag{D 12}$$

REFERENCES

ALLEN, J. S. 1991 Balance equations based on momentum equations with global invariants of potential enstrophy and energy. *J. Phys. Oceanogr.* **21**, 265–276.

ALLEN, J. S. 1993 Iterated geostrophic intermediate models. *J. Phys. Oceanogr.* **23** (1), 2447–2461.

ALLEN, J. S., BARTH, J. A. & NEWBERGER, P. A. 1990*a* On intermediate models for barotropic continental shelf and slope flow fields. Part i. Formulation and comparison of exact solutions. *J. Phys. Oceanogr.* **20**, 1017–1042.

ALLEN, J. S., BARTH, J. A. & NEWBERGER, P. A. 1990*b* On intermediate models for barotropic continental shelf and slope flow fields. Part iii. Comparison of numerical model solutions in periodic channels. *J. Phys. Oceanogr.* **20** (2), 1949–1973.

ALLEN, J. S. & NEWBERGER, P. A. 1993 On intermediate models for stratified flow. *J. Phys. Oceanogr.* **23** (2), 2462–2485.

BABIN, A., MAHALOV, A. & NICOLAENKO, B. 2000 Fast singular oscillating limits and global regularity for the three-dimensional primitive equations of geophysics. *Math. Model. Num. Anal.* **34**, 201–222.

BABIN, A., MAHALOV, A. & NICOLAENKO, B. 2002 Singular oscillating limits of stably-stratified three-dimensional euler and Navier–Stokes equations and a geostrophic wave fronts. In *Large-Scale Atmosphere-Ocean Dynamics I* (ed. J. Norbury & I. Rhoulstone). Cambridge University Press.

BARTELLO, P. 1995 Geostrophic adjustment and inverse cascades in rotating stratified turbulence. *J. Atmos. Sci.* **52**, 4410–4428.

BARTH, J. A., ALLEN, J. S. & NEWBERGER, P. A. 1990 On intermediate models for barotropic continental shelf and slope flow fields. Part ii. Comparison of numerical model solutions in doubly periodic domains. *J. Phys. Oceanogr.* **20**, 1044–1076.

CHARNEY, J. G. 1948 On the scale of atmospheric motions. *Geofysiske Publikasjoner* **17** (2), 1–17.

EMBID, P. F. & MAJDA, A. J. 1996 Averaging over fast gravity waves for geophysical flows with arbitrary potential vorticity. *Comm. Partial Diff. Eq.* **21** (3–4), 619–658.

EMBID, P. F. & MAJDA, A. J. 1998 Low Froude number limiting dynamics for stably stratified flow with small or finite Rossby numbers. *Geophys. Astrophys. Fluid Dyn.* **87** (1–2), 1–50.

FARGE, M. & SADOURNY, R. 1989 Wave-vortex dynamics in rotating shallow water. *J. Fluid Mech.* **206**, 433–462.

FORD, R., McINTYRE, M. E. & NORTON, W. A. 2000 Balance and the slow quasimanifold: some explicit results. *J. Atmos. Sci.* **57**, 1236–1254.

HAKIM, G. J., SNYDER, C. & MURAKI, D. J. 2002 A new surface model for cyclone–anticyclone asymmetry. *J. Atmos. Sci.* **59**, 2405–2420.

JULIEN, K., KNOBLOCH, E., MILLIFF, R. & WERNE, J. 2006 Generalized quasi-geostrophy for spatially anisotropic rotationally constrained flows. *J. Fluid Mech.* **555**, 233–274.

KRAICHNAN, R. H. 1973 Helical turbulence and absolute equilibrium. *J. Fluid Mech.* **59**, 745–752.

KUNDU, P. K. & COHEN, I. M. 2004 *Fluid Mechanics*. Academic Press.

KUO, A. C. & POLVANI, L. M. 1999 Wave–vortex interaction in rotating shallow water. I. One space dimension. *J. Fluid Mech.* **394**, 1–27.

KUO, A. C. & POLVANI, L. M. 2000 Nonlinear geostrophic adjustment, cyclone/anticyclone asymmetry, and potential vorticity rearrangement. *Phys. Fluids* **12** (5), 1087–1100.

LORENZ, E. N. 1960 Energy and numerical weather prediction. *Tellus* **4**, 364–373.

MAJDA, A. & EMBID, P. 1998 Averaging over fast gravity waves for geophysical flows with unbalanced initial data. *Theor. Comput. Fluid Dyn.* **11**, 155–169.

MAJDA, A. 2003 *Introduction to PDEs and Waves for the Atmosphere and Ocean*. Courant Lecture Notes in Mathematics, vol. 9. New York University, Courant Institute of Mathematical Sciences.

MALTRUD, M. E. & VALLIS, G. K. 1990 Energy spectra and coherent structures in forced two-dimensional and beta-plane turbulence. *J. Fluid Mech.* **228**, 321–342.

MARTIN, JONATHAN E. 2006 *Mid-Latitude Atmospheric Dynamics: A First Course*. Wiley.

McINTYRE, M. E. & NORTON, W. A. 2000 Potential vorticity inversion on a hemisphere. *J. Atmos. Sci.* **57** (9), 1214–1235.

McWILLIAMS, J. C. 1984 The emergence of isolated coherent vortices in turbulent flow. *J. Fluid Mech.* **146**, 21–43.

McWILLIAMS, J. C. & GENT, P. R. 1980 Intermediate models of planetary circulations in the atmosphere and ocean. *J. Atmos. Sci.* **37** (8), 1657–1678.

MOHEBALHOJEH, A. R. & DRITSCHEL, D. G. 2001 Hierarchies of balance conditions for the f-plane shallow water equations. *J. Atmos. Sci.* **58**, 2411–2426.

MURAKI, D. J. & HAKIM, G. J. 2001 Balanced asymmetries of waves on the tropopause. *J. Atmos. Sci.* **58**, 237–252.

MURAKI, D., SNYDER, C. & ROTUNNO, R. 1999 The next-order corrections to quasigeostrophic theory. *J. Atmos. Sci.* **56**, 1547–1560.

OBUKHOV, A. M. 1949 On the problem of geostrophic wind. *Izv. Geogr. Geophys.* **13**, 281–306 (in Russian).

PEDLOSKY, J. 1986 *Geophysical Fluid Dynamics*. Springer-Verlag.

POLVANI, L., MCWILLIAMS, J., SPALL, M. & FORD, R. 1994 The coherent structures of shallow-water turbulence: deformation radius effects, cyclone/anticyclone asymmetry and gravity-wave generation. *Chaos* **4**, 177–186.

REZNIK, G. M., ZEITLIN, V. & BEN JELLOUL, M. 2001 Nonlinear theory of geostrophic adjustment. Part 1. Rotating shallow-water model. *J. Fluid Mech.* **445**, 93–120.

ROTUNNO, R., MURAKI, D. & SNYDER, C. 2000 Unstable baroclinic waves beyond quasigeostrophic theory. *J. Atmos. Sci.* **57**, 3285–3295.

SADOURNY, R. 1975 The dynamics of finite-difference models of the shallow-water equations. *J. Atmos. Sci.* **32**, 680–689.

SALMON, R. 1998 *Lectures on Geophysical Fluid Dynamics*. Oxford University Press.

SMITH, L. M. & WALEFFE, F. 2002 Generation of slow, large scales in forced rotating, stratified turbulence. *J. Fluid Mech.* **451**, 145–168.

SPALL, M. A. & MCWILLIAMS, J. C. 1992 Rotational and gravitational influences on the degree of balance in the shallow-water equations. *Geophys. Astrophys. Fluid Dyn.* **64**, 1–29.

STEGNER, A. & ZEITLIN, V. 1995 What can asymptotic expansions tell us about large-scale quasi-geostrophic anticyclonic vortices? *Nonlinear Process. Geophys.* **2** (3/4), 186–193.

SUKHATME, J. & SMITH, L. 2008 Vortical and wave modes in three-dimensional rotating stratified flows: random large-scale forcing. *Geophys. Astrophys. Fluid Dyn.* **102** (19), 437–455.

VALLIS, G. K. 1996 Potential vorticity inversion and balanced equations of motion for rotating and stratified flows. *Q. J. Royal Meteorol. Soc.* **122**, 291–322.

WAITE, M. L. & BARTELLO, P. 2006 The transition from geostrophic to stratified turbulence. *J. Fluid Mech.* **568**, 89–108.

WARN, T. 1986 Statistical mechanical equilibria of the shallow water equations. *Tellus Ser. Dynamic Meteorol. Oceanogr.* **38**, 1–11.

WARN, T., BOKHOVE, O., SHEPHERD, T. G. & VALLIS, G. K. 1995 Rossby number expansions, slaving principles and balance dynamics. *Q. J. Royal Meteorol. Soc.* **121**, 723–739.

YAVNEH, I. & MCWILLIAMS, J. C. 1994 Breakdown of the slow manifold in the shallow-water equations. *Geophys. Astrophys. Fluid Dyn.* **75**, 131–161.

YUAN, L. & HAMILTON, K. 1994 Equilibrium dynamics in a forced-dissipative f-plane shallow-water system. *J. Fluid Mech.* **280**, 369–394.